AERO. & ASTRO. LIBRARY

MASS. INST. OF TECHNOLOGY
AERO.
ENGINEERING LIBRARY

NATIONAL ADVISORY COMMITTEE FOR AERONAUTICS

REPORT No. 646

c. 3

THE COMPRESSIBILITY BURBLE AND THE EFFECT OF COMPRESSIBILITY ON PRESSURES AND FORCES ACTING ON AN AIRFOIL

By JOHN STACK, W. F. LINDSEY, and ROBERT E. LITTELL

1938

For sale by the Superintendent of Documents, Washington, D. C. - - - - - - - - - - - - - - Price 15 cents
Subscription price, $3.00 per year

AERONAUTIC SYMBOLS

1. FUNDAMENTAL AND DERIVED UNITS

	Symbol	Metric		English	
		Unit	Abbreviation	Unit	Abbreviation
Length	l	meter	m	foot (or mile)	ft. (or mi.)
Time	t	second	s	second (or hour)	sec. (or hr.)
Force	F	weight of 1 kilogram	kg	weight of 1 pound	lb.
Power	P	horsepower (metric)		horsepower	hp.
Speed	V	kilometers per hour	k.p.h.	miles per hour	m.p.h.
		meters per second	m.p.s.	feet per second	f.p.s.

2. GENERAL SYMBOLS

W, Weight$=mg$

g, Standard acceleration of gravity$=9.80665$ m/s^2 or 32.1740 ft./sec.^{2}

m, Mass$=\frac{W}{g}$

I, Moment of inertia$=mk^2$. (Indicate axis of radius of gyration k by proper subscript.)

μ, Coefficient of viscosity

ν, Kinematic viscosity

ρ, Density (mass per unit volume)

Standard density of dry air, 0.12497 kg-m^{-4}-s^2 at 15° C. and 760 mm; or 0.002378 lb.-ft.$^{-4}$ sec.^{2}

Specific weight of "standard" air, 1.2255 kg/m^3 or 0.07651 lb./cu. ft.

3. AERODYNAMIC SYMBOLS

S, Area

S_w, Area of wing

G, Gap

b, Span

c, Chord

$\frac{b^2}{S}$, Aspect ratio

V, True air speed

q, Dynamic pressure$=\frac{1}{2}\rho V^2$

L, Lift, absolute coefficient $C_L=\frac{L}{qS}$

D, Drag, absolute coefficient $C_D=\frac{D}{qS}$

D_0, Profile drag, absolute coefficient $C_{D_0}=\frac{D_0}{qS}$

D_i, Induced drag, absolute coefficient $C_{D_i}=\frac{D_i}{qS}$

D_p, Parasite drag, absolute coefficient $C_{D_p}=\frac{D_p}{qS}$

C, Cross-wind force, absolute coefficient $C_C=\frac{C}{qS}$

R, Resultant force

i_w, Angle of setting of wings (relative to thrust line)

i_t, Angle of stabilizer setting (relative to thrust line)

Q, Resultant moment

Ω, Resultant angular velocity

$\rho\frac{Vl}{\mu}$, Reynolds Number, where l is a linear dimension (e.g., for a model airfoil 3 in. chord, 100 m.p.h. normal pressure at 15° C., the corresponding number is 234,000; or for a model of 10 cm chord, 40 m.p.s., the corresponding number is 274,000)

C_p, Center-of-pressure coefficient (ratio of distance of c.p. from leading edge to chord length)

α, Angle of attack

ϵ, Angle of downwash

α_0, Angle of attack, infinite aspect ratio

α_i, Angle of attack, induced

α_a, Angle of attack, absolute (measured from zero-lift position)

γ, Flight-path angle

REPORT No. 646

THE COMPRESSIBILITY BURBLE AND THE EFFECT OF COMPRESSIBILITY ON PRESSURES AND FORCES ACTING ON AN AIRFOIL

By JOHN STACK, W. F. LINDSEY, and ROBERT E. LITTELL
Langley Memorial Aeronautical Laboratory

104360—39——1

NATIONAL ADVISORY COMMITTEE FOR AERONAUTICS

HEADQUARTERS, NAVY BUILDING, WASHINGTON, D. C.

LABORATORIES, LANGLEY FIELD, VA.

Created by act of Congress approved March 3, 1915, for the supervision and direction of the scientific study of the problems of flight (U. S. Code, Title 50, Sec. 151). Its membership was increased to 15 by act approved March 2, 1929. The members are appointed by the President, and serve as such without compensation.

JOSEPH S. AMES, Ph. D., *Chairman*,
Baltimore, Md.
DAVID W. TAYLOR, D. Eng., *Vice Chairman*,
Washington, D. C.
WILLIS RAY GREGG, Sc. D., *Chairman, Executive Committee*,
Chief, United States Weather Bureau.
WILLIAM P. MACCRACKEN, J. D., *Vice Chairman, Executive Committee*,
Washington, D. C.
CHARLES G. ABBOT, Sc. D.,
Secretary, Smithsonian Institution.
LYMAN J. BRIGGS, Ph. D.,
Director, National Bureau of Standards.
ARTHUR B. COOK, Rear Admiral, United States Navy,
Chief, Bureau of Aeronautics, Navy Department.
HARRY F. GUGGENHEIM, M. A.,
Port Washington, Long Island, N. Y.
SYDNEY M. KRAUS, Captain, United States Navy,
Bureau of Aeronautics, Navy Department.
CHARLES A. LINDBERGH, LL. D.,
New York City.
DENIS MULLIGAN, J. S. D.,
Director of Air Commerce, Department of Commerce.
AUGUSTINE W. ROBINS, Brigadier General, United States Army,
Chief Matériel Division, Air Corps, Wright Field, Dayton, Ohio.
EDWARD P. WARNER, Sc. D.,
Greenwich, Conn.
OSCAR WESTOVER, Major General, United States Army,
Chief of Air Corps, War Department.
ORVILLE WRIGHT, Sc. D.,
Dayton, Ohio.

GEORGE W. LEWIS, *Director of Aeronautical Research*

JOHN F. VICTORY, *Secretary*

HENRY J. E. REID, *Engineer-in-Charge, Langley Memorial Aeronautical Laboratory, Langley Field, Va.*

JOHN J. IDE, *Technical Assistant in Europe, Paris, France*

TECHNICAL COMMITTEES

AERODYNAMICS
POWER PLANTS FOR AIRCRAFT
AIRCRAFT MATERIALS
AIRCRAFT STRUCTURES
AIRCRAFT ACCIDENTS
INVENTIONS AND DESIGNS

Coordination of Research Needs of Military and Civil Aviation

Preparation of Research Programs

Allocation of Problems

Prevention of Duplication

Consideration of Inventions

LANGLEY MEMORIAL AERONAUTICAL LABORATORY

LANGLEY FIELD, VA.

Unified conduct, for all agencies, of scientific research on the fundamental problems of flight.

OFFICE OF AERONAUTICAL INTELLIGENCE

WASHINGTON, D. C.

Collection, classification, compilation, and dissemination of scientific and technical information on aeronautics.

REPORT No. 646

THE COMPRESSIBILITY BURBLE AND THE EFFECT OF COMPRESSIBILITY ON PRESSURES AND FORCES ACTING ON AN AIRFOIL

By John Stack, W. F. Lindsey, and Robert E. Littell

SUMMARY

Simultaneous air-flow photographs and pressure-distribution measurements were made of the N. A. C. A. 4412 airfoil at high speeds to determine the physical nature of the compressibility burble. The tests were conducted in the N. A. C. A. 24-inch high-speed wind tunnel. The flow photographs were obtained by the schlieren method and the pressures were simultaneously measured for 54 stations on the 5-inch-chord airfoil by means of a multiple-tube manometer. Following the general program, a few measurements of total-pressure loss in the wake of the airfoil at high speeds were made to illustrate the magnitude of the losses involved and the extent of the disturbed region; and, finally, in order to relate this work to earlier force-test data, a force test of a 5-inch-chord N. A. C. A. 4412 airfoil was made.

The data presented include the results of pressure-distribution measurements and force tests for three low angles of attack for a speed range extending from one-tenth the speed of sound to speeds in excess of the critical values at which a breakdown of the flow, or compressibility burble, occurs.

The results show the general nature of the phenomenon known as the compressibility burble. The source of the increased drag is shown to be a compression shock that occurs on the airfoil as its speed approaches the speed of sound. Finally, it is indicated that considerable experimentation is needed in order to understand the phenomenon completely.

INTRODUCTION

The development of the knowledge of compressible-flow phenomena, particularly as related to aeronautical applications, has been attended by considerable difficulty. The complicated nature of the phenomena has resulted in little theoretical progress and, in general, recourse to experiment has been necessary. Until recently the most important experimental results have been obtained in connection with the science of ballistics, but this information has been of little value in aeronautical problems because the range of speeds for which most ballistic experiments have been made extends from the speed of sound upward; whereas, the important region in aeronautics at the present time extends from the speed of sound downward. Studies of flow in nozzles have yielded some valuable results, although the available data do not appear to allow a reliable prediction of the air-flow phenomena associated with airfoils. Previous published aeronautical experiments have generally consisted of measurements of the forces experienced by airfoil sections and propellers at high speeds. These data demonstrate that serious detrimental flow changes may occur as speeds approach the speed of sound but have not shown the character of such flow changes.

The principal result of the propeller tests appears to be the establishment of the critical speeds for many standard blades. The force tests of airfoils have permitted a wider interpretation of the propeller data and have indicated the effects of certain shape changes on the value of the critical speed. The theory of Glauert and Ackeret has been substantiated in fair degree by airfoil tests for speeds below the critical, but their theory gives no clue as to any flow changes that may occur. This deficiency is important because tests of both airfoils and propellers have shown the existence of a critical speed above which resistance to motion becomes impracticably large. Taylor's electric analogy appears to give the best indication of the speed at which these flow changes occur but gives little insight into the phenomena.

It therefore appeared that the nature of the flow changes must be discovered in order to explain the compressibility effects which have been measured in previous experiments. A research program was outlined to obtain this information, to establish the limitations of available theoretical work, and to obtain information upon which developments of practical significance for aeronautical applications could be based. The proposed experiments included pressure-distribution measurements for a typical airfoil and flow-visualization experiments.

Preliminary flow observations by the schlieren method were originally made for a cylinder and an N. A. C. A. 0012 airfoil in the N. A. C. A. 11-inch high-speed wind tunnel. The observations with the airfoil were correlated with previous force tests and the results were first shown at the N. A. C. A. Engineering Research Conference in 1934. A more general program was then formulated that included pressure-distribu-

tion measurements and schlieren photographs. These experiments were made in the N. A. C. A. 24-inch high-speed wind tunnel with an N. A. C. A. 4412 airfoil section of 5-inch chord. After the main program had been completed, some additional tests were made to study the magnitude of the energy losses associated with high-speed flows; these tests comprised measurements of the total-pressure loss that occurred in the compression shock, which was shown to exist in the flow. In order to correlate the data with previous

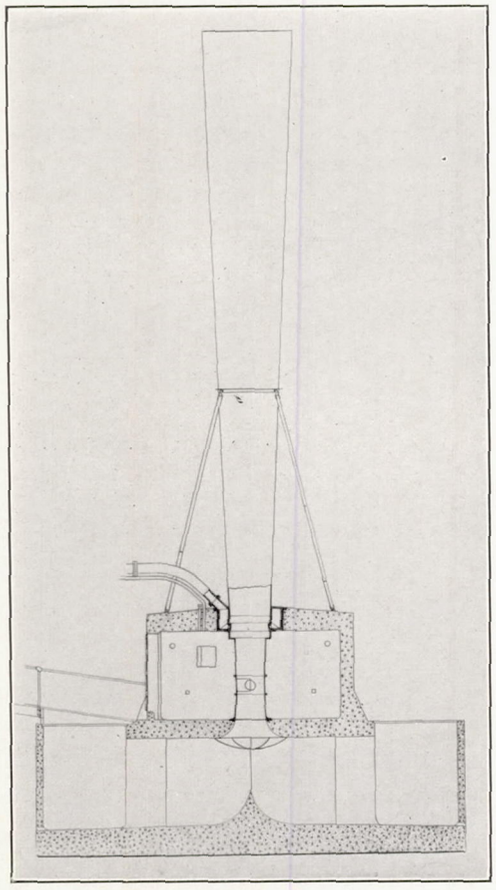

FIGURE 1.—Longitudinal section of the N. A. C. A. 24-inch high-speed wind tunnel.

work, force tests of a 5-inch-chord N. A. C. A. 4412 airfoil were also made.

Most of the experiments were carried out during 1935 and 1936. All the tests were made in the N. A. C. A. 24-inch high-speed wind tunnel. Some of the outstanding results have been published in preliminary form as references 1 and 2.

APPARATUS AND METHOD

The N. A. C. A. 24-inch high-speed wind tunnel (fig. 1) in which this investigation was conducted is an induction-type wind tunnel. Compressed air from the variable-density wind tunnel discharged through an annular nozzle located downstream from the test section induces a flow of air from the atmosphere through the test section. Velocities approaching the speed of sound may be obtained at the test section. The tunnel is located outside the building that houses the variable-density wind tunnel. Except for certain modifications arising from its outside location and its size, the methods of operation are the same as for the 11-inch high-speed wind tunnel (reference 3). The essential air passages are geometrically similar to those of the 11-inch high-speed wind tunnel, and the general air-stream characteristics of the tunnel are equivalent to those of the 11-inch tunnel except for the static-pressure gradient, which is zero.

The method for flow observations and photography is the schlieren method devised by Töpler; the fundamental principles are described in reference 4. A simplified diagram of the apparatus used in these experiments is given in figure 2. Light from a source located at C, the principal focus of lens D, emerges from lens D as a parallel beam, passes through the converging lens D′, and is brought to focus at E, the

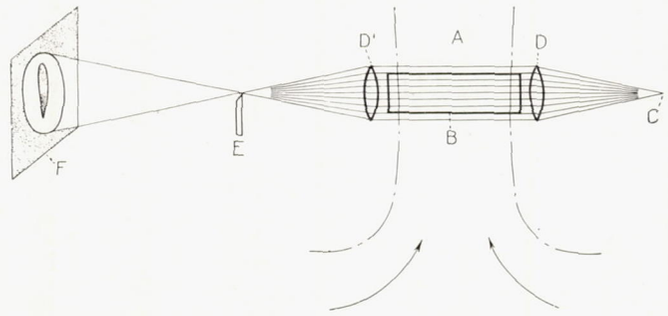

FIGURE 2.—Simplified diagram showing the schlieren method.

principal focus of lens D′. At E a knife edge is located so as to cut off most of the light from the source C. The model B is placed in the parallel beam that crosses the test section A between the lenses so that its cross section is perpendicular to the light beam and an image is formed on the screen F. When air passes over the model, its density, and therefore its optical index of refraction, change. Thus, portions of the parallel beam of light are bent and some of the rays that were previously interrupted by the knife edge now pass over the knife edge at E to the screen F or, if desired, to a photographic plate. The illumination on the screen then shows regions of varying density.

For these experiments the source light was a high-intensity spark. Lenses D and D′ are of 5-inch diameter and 26-inch focal length. The screen F was replaced by a photographic plate mounted in a standard 8- by 10-inch studio-type camera from which the lens had been removed. The camera was mounted so that

the shutter was near the knife edge; photographic operation was then similar to the methods normally used in making photographs. Because of the small diameter of the lenses in relation to the airfoil chord, it was necessary to use the full field of the lenses; and, further, because of the curved transparent wall sections by which the model was supported (described later), the resulting pictures, particularly near the leading and the trailing edges of the model, are not of high quality. The results obtained, however, are satisfactory in that they illustrate clearly the type of phenomenon which occurs.

The pressures acting on the airfoil were measured by means of a multiple-tube photorecording manometer described in detail in reference 5. The manometer contains 60 tubes arranged in a semicircle with a neon light parallel to the tubes located at the center of the semicircle. Photostat paper is drawn from a roll, located at the back of the manometer, around the tubes; and the exposed lengths of paper are drawn up on another roll also located at the back of the manometer. A mechanism for automatic remote control is contained within the manometer. During the tests three manometer liquids were used: mercury for high speeds, tetrabromoethane (specific gravity, approximately 3) for medium speeds, and alcohol for low speeds.

The N. A. C. A. 4412 rectangular airfoil of 5-inch chord and 30-inch span consists of a brass center section of 1-inch span and duralumin end pieces. Fifty-four holes are arranged in two rows, one-fourth inch apart, along the upper and the lower surfaces at the center of the brass section. These holes were connected to the manometer by small brass tubes led out through two large ducts in the lower surface of the duralumin end pieces of the model. The ducts were closed by duralumin covers shaped to the contour of the airfoil. The brass center section and the duralumin end pieces were bolted together and all joints were carefully made to preserve the contour and fairness of the model. A more detailed description of this model is given in reference 5.

Mounted for tests, the airfoil extended through the tunnel walls and was supported in carefully fitted celluloid end plates that preserved the contour of the tunnel wall. The model was originally designed for tests in the variable-density wind tunnel where the supporting system is such that the bending stresses at the center of the model resulting from lift loads are small. For some of the tests in the high-speed wind tunnel, it was necessary to provide auxiliary bracing to support the lift loads because of the inherent structural weakness of the model at the center section. This bracing consisted of cables secured at the quarter-chord point of the airfoil approximately 6 inches out from the center on either side and fastened to the tunnel wall. These cables appear in some of the schlieren photographs as dark lines extending outward from the airfoil approximately perpendicular to the lower surface; they should not be confused with the compression shock.

The operation of the apparatus was controlled from outside because of the large rate of pressure change within the tunnel chamber as the air speed was rapidly varied. The test procedure consisted in first increasing the speed to the desired value by a motor-driven valve in the compressed-air supply line; the speed was measured by an outside mercury manometer connected to calibrated static plates. The camera shutter, which was operated by an electromagnet, was then opened and, at a signal immediately following, the electric circuit for the manometer light and the source light in the schlieren apparatus were closed. By this procedure the pressure record and the flow photograph were simultaneously obtained.

Supplementary tests.—After the completion of the original program, some additional tests consisting of measurements of total-pressure loss behind the airfoil and force tests of a 5-inch-chord duralumin airfoil were made. For the measurements of total-pressure loss, the individual tubes of a rake of impact tubes were connected to a manometer and the pressure distribution and the total-pressure loss were simultaneously measured. Owing to insufficient manometer equipment, these tests were incomplete and the pressure data include, except for one series of tests, the measurements of pressure distribution and total-pressure loss for only the upper surface of the model. Furthermore, the schlieren apparatus had by this time been dismantled so that no flow photographs were made.

The rake of impact tubes was made of 19 tubes and extended from the tunnel wall to a point three-fourths inch past the quarter-chord axis of the model. The forward ends of the tubes were located one-half inch behind the trailing edge of the model. The locations of the tubes are shown by the points on the plots (figs. 18 to 20). Because of the relatively large spacing of the tubes and the insufficient manometer equipment, total-pressure losses for low speeds could not be accurately obtained and the data as presented show only the loss that occurred at high speeds after a compression shock had formed. As previously noted, these measurements were made after the main program had been completed and are exploratory in nature. The results should therefore be considered mainly for qualitative purposes.

The force tests of a 5-inch-chord all-duralumin airfoil were made in the manner described in reference 3. A complete description of this model is given in reference 6. One important difference between the methods employed for the pressure-distribution tests and the force

tests was the manner in which the models were mounted. For the force tests, the model was mounted on the balance and extended across the tunnel, passing through holes, which were of the same shape as but slightly larger than the model, cut in flexible brass end plates that preserved the contour of the tunnel walls. Thus, leakage of air occurred around the model ends. The pressure-distribution model was tested before the installation of the balance and was supported by the end plates; the consequent tight fit permitted no appreciable end leakage.

The balance, except for improvements that permit a more accurate determination of the forces, is similar in principle to the one used in the 11-inch high-speed wind tunnel and the methods of operation are likewise similar to those employed in the operation of the 11-inch tunnel (reference 3).

Range of tests.—The speed range over which measurements were made extended, in general, from one-tenth the speed of sound to values in excess of the critical speed. The corresponding Reynolds Number range was from approximately 350,000 to nearly 2,000,000. Tests were made for only small angles of attack because the primary purpose of the experiments, to discover the nature of the flow phenomena at the critical speed, could be accomplished at small angles of attack, and further, the extension of the tests to higher angles of attack would add a considerable amount of work without, it was felt, adding materially to the fundamental significance of the results obtained. In the supplementary tests, the force measurements were made for the speed range and the angle-of-attack range previously noted, but the pressure-loss measurements were made only for speeds in the critical region.

RESULTS

The following symbols are used in this report:

c, speed of sound.
V, speed of the general air stream.
u, local velocity of the air stream.
u_1, local velocity in front of the compression shock.
u_2, local velocity behind the compression shock.
ρ_1, density in front of the compression shock.
ρ_2, density behind the compression shock.
M, compressibility index, V/c.
γ, specific-heat ratio; value taken, 1.4.
p_a, atmospheric pressure.
p, static pressure in the free stream.
p_l, local static pressure (as at airfoil surface).
p_1, airfoil surface pressure in front of the compression shock.
p_2, airfoil surface pressure behind the compression shock.
P, pressure coefficient, $(p_l-p)/q$ (the ordinate of the pressure-distribution diagram).
P_0, pressure coefficient for imcompressible flow.
P_c, critical-pressure coefficient, that is, the pressure coefficient corresponding to the local velocity of sound $(0.528\ p_a-p)/q$.
H, total pressure (or impact pressure). Free-stream value of H equals p_a for the 24-inch high-speed wind tunnel.
H_1, total pressure in front of the compression shock.
H_2, total pressure behind the compression shock.
r/c, distance from leading edge in percent of chord.

The test data have been reduced to standard nondimensional form. The dynamic pressure q and the compressibility index M were determined by measurements of the pressures at calibrated static-pressure orifices in the tunnel wall. These orifices were connected to the photorecording manometer and, like the pressures acting on the surfaces of the airfoil, the orifice pressures were determined by measuring the deflections of the liquid in the manometer tubes as shown on the photographic records. A detailed description of the method for computing q and M is given in reference 3.

The pressure-distribution data are presented in figures 3 to 5. Figures 6 to 8 are schlieren photographs, each of which corresponds to one of the pressure-distribution diagrams given in figures 3 to 5. Plots of the airfoil characteristics (lift coefficient C_L, drag coefficient C_D, and pitching-moment coefficient $C_{m_{c/4}}$) obtained from integrations of the pressure distribution and the force-test data are presented in figures 9 to 11 in a form that illustrates the effect of compressibility. Some of the more significant local effects of compressibility are shown in figures 12 to 14. Figure 15 is included to illustrate the effect that variations in Reynolds Number may have on the local pressures.

The magnitude of the energy losses in the flow that give rise to the large drag increases at high speeds is illustrated by figure 17. Figures 18 to 21 show the loss in total pressure behind the compression shock that occurs at high speeds. In figure 22 a curve from which the critical speed may be estimated is given and comparisons with the test data are included.

PRECISION

Inaccuracies arising from variations of the dynamic pressure, directional variation of the flow across the test section, and static-pressure gradient are insignificant. The tunnel-wall effect, however, is important, particularly as related to the comparison of the results of force and pressure-distribution tests. In the pressure-distribution tests, the tight juncture of the model and the tunnel wall permitted no appreciable end leakage and, furthermore, measurements were made only at the center section of the model; as a result, the

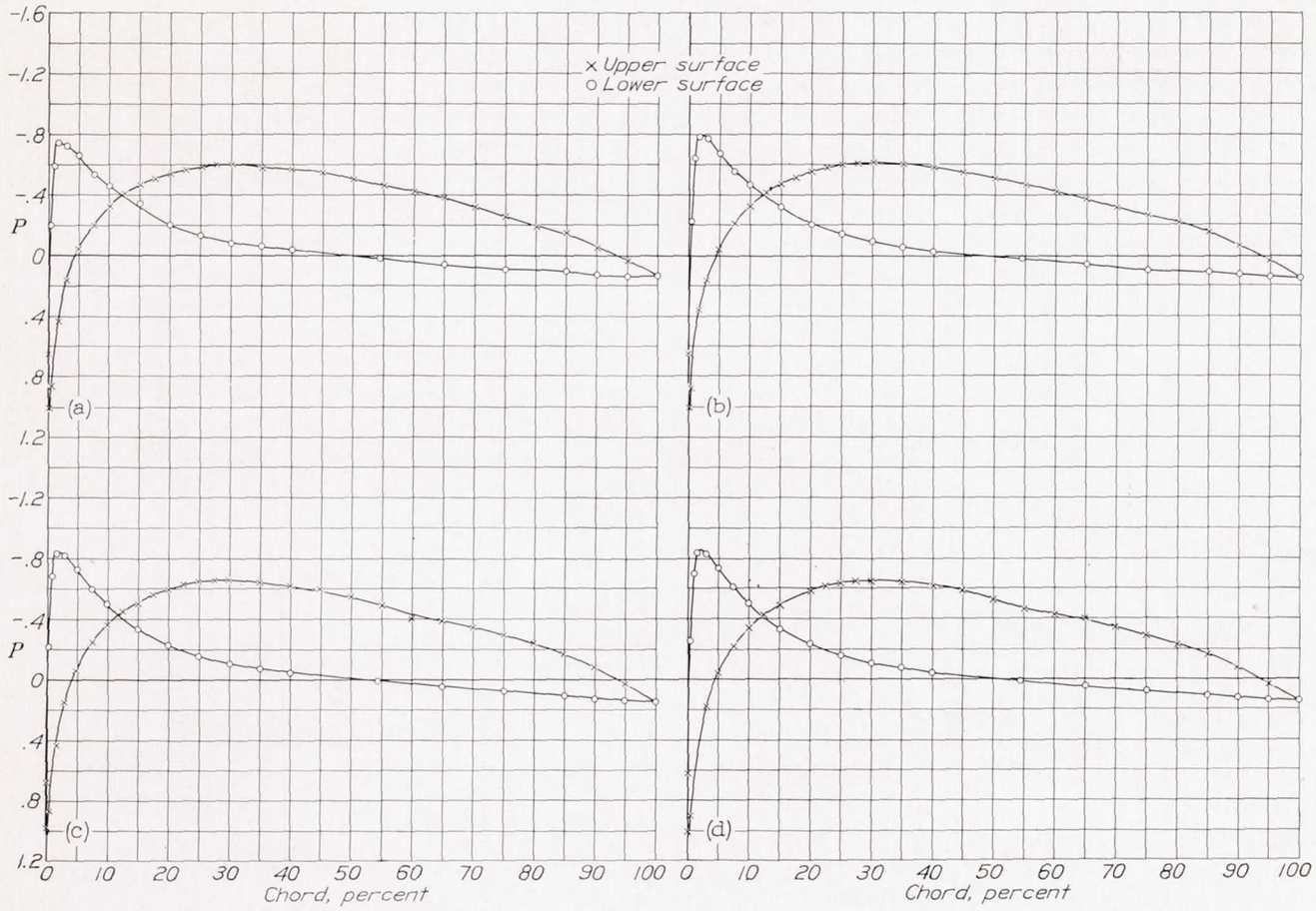

(a) $M=0.100$; test 24–25.
(b) $M=0.186$; test 24–26.
(c) $M=0.297$; test 24–20.
(d) $M=0.334$; test 24–25.

FIGURE 3.—Pressure distribution for the N. A. C. A. 4412 airfoil. $\alpha=-2°$.

data closely approximate those for two-dimensional flow. For the force tests, however, there was a small clearance where the model passed through the tunnel walls, which appears, from preliminary investigations, to necessitate an important correction for leakage as well as for tunnel-wall effect.

Other errors are indicated by the scatter of the points on the curves. For the pressure-distribution data, figures 3(f), 3(k), 4(c), and 4(f) show that, for low speeds, the accidental error is negligible; but, at speeds approaching and beyond the critical, the error is increased owing to the flow unsteadiness caused by the compression shock. Integrations of the pressure-distribution diagrams are subject to additional errors arising from variations in the fairing of the curves, particularly in the region where compression shock may occur, and the magnitude of these errors is included in the point scatter in figure 9.

Errors in the integrated values of total-pressure loss may be large owing to the small number of measurements made in the wake of the wing and the corresponding uncertainty in the drawing of the curves. These data, however, are intended to show qualitatively the magnitude of the loss and quantitatively the extent of the flow disturbance at the compressibility burble. When the data are used for these purposes, the errors are insignificant.

Balance calibrations before and after the force tests agreed very closely. In general, force-test results can be repeated to within 3 percent.

Further errors may arise from variations in the static-plate calibrations and the effect of atmospheric humidity. For these tests, however, there were no measurable changes in the static-plate calibrations, which were repeated several times during the progress of the tests. Humidity effects under certain conditions may be large because of the high expansion and the consequent lowering of temperature that occurs as the air is accelerated to the high speeds attained in the high-speed wind tunnel. Preliminary tests, however, indicated a value of the relative humidity below which no measurable effects occurred and most of the data were therefore taken for humidity conditions corresponding to the region in which no effects could be measured. A small amount of the data was taken at conditions exceeding the indicated limit, but the errors are included in the scatter of the test points.

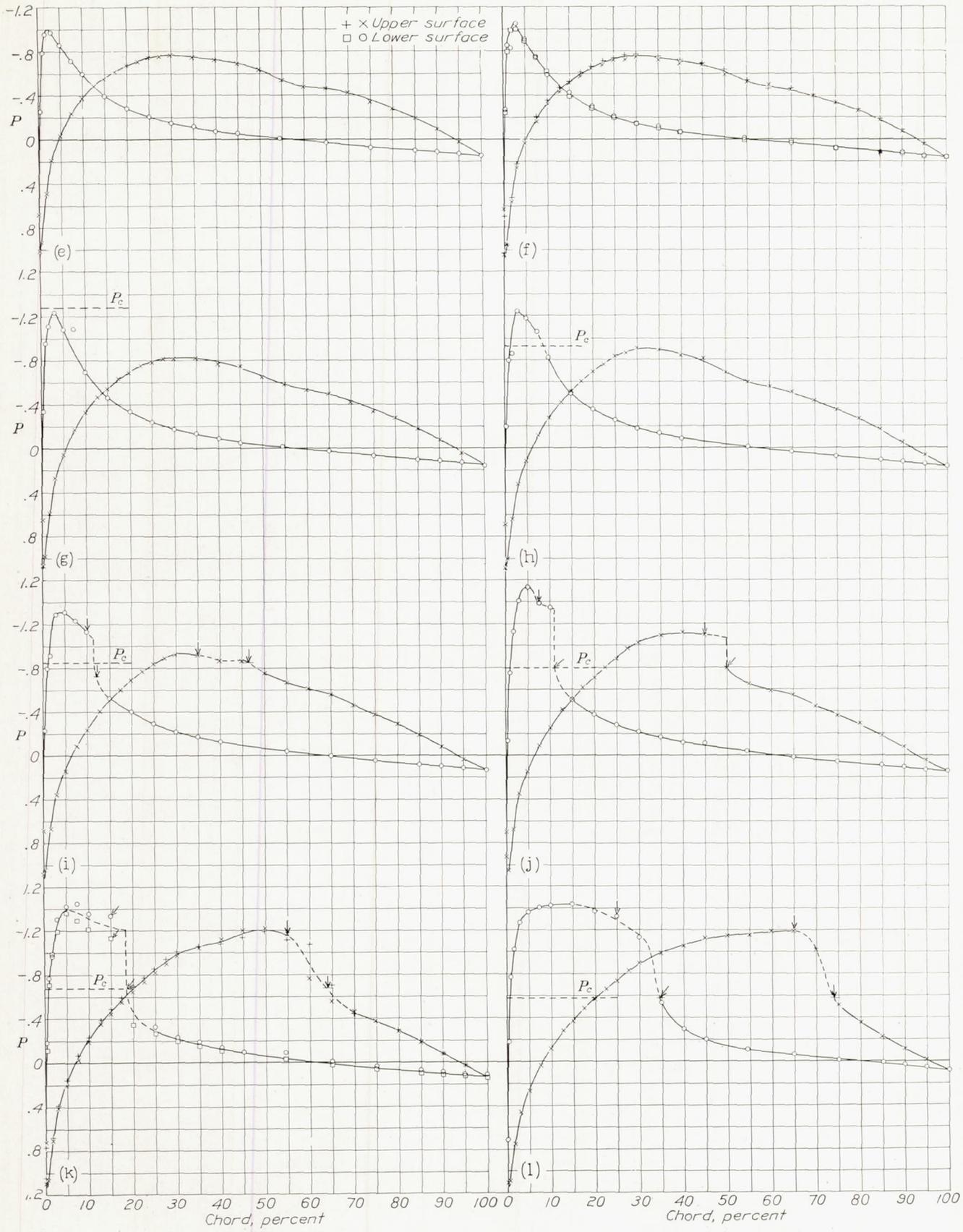

(e) $M=0.498$; test 24-20.
(g) $M=0.603$; test 24-12.
(i) $M=0.683$; test 24-12.
(k) ×○$M=0.726$; test 24-12.
+□$M=0.727$; test 24-22.

(f) ×○$M=0.534$; test 24-12.
+□$M=0.533$; test 24-20.
(h) $M=0.668$; test 24-12.
(j) $M=0.696$; test 24-12.
(l) $M=0.756$; test 24-12.

FIGURE 3.—Pressure distribution for the N. A. C. A. 4412 airfoil. $\alpha=-2°$—Continued.

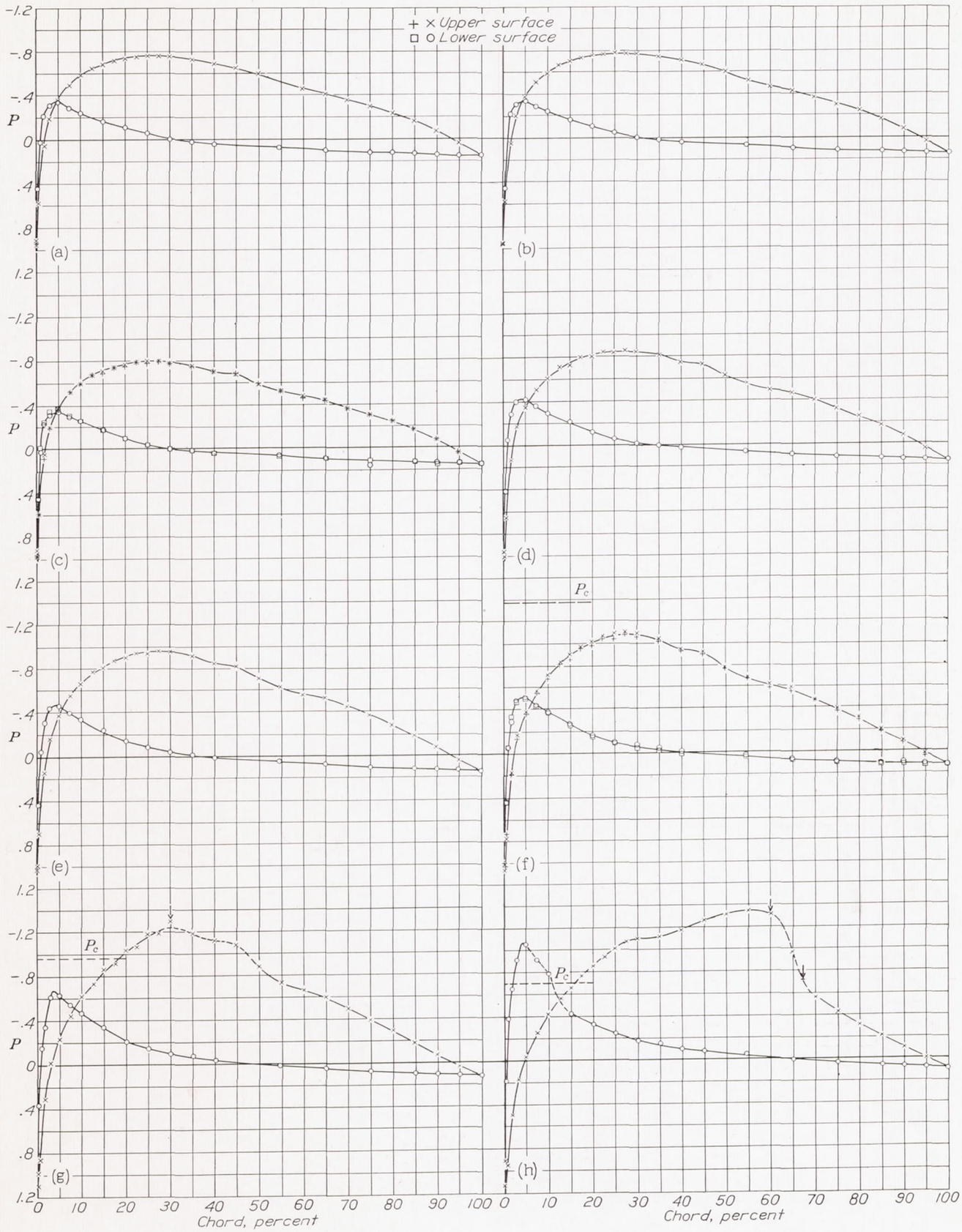

(a) $M=0.141$; test 24-26.
(c) ×○$M=0.299$; test 24-25.
+□$M=0.298$; test 24-21.
(e) $M=0.517$; test 24-21.
(g) $M=0.659$; test 24-12.

(b) $M=0.206$; test 24-26.
(d) $M=0.427$; test 24-21.
(f) ×○$M=0.590$; test 24-12.
+□$M=0.589$; test 24-21.
(h) $M=0.717$; test 24-12.

FIGURE 4.—Pressure distribution for the N. A. C. A. 4412 airfoil. $\alpha=-0°15'$.

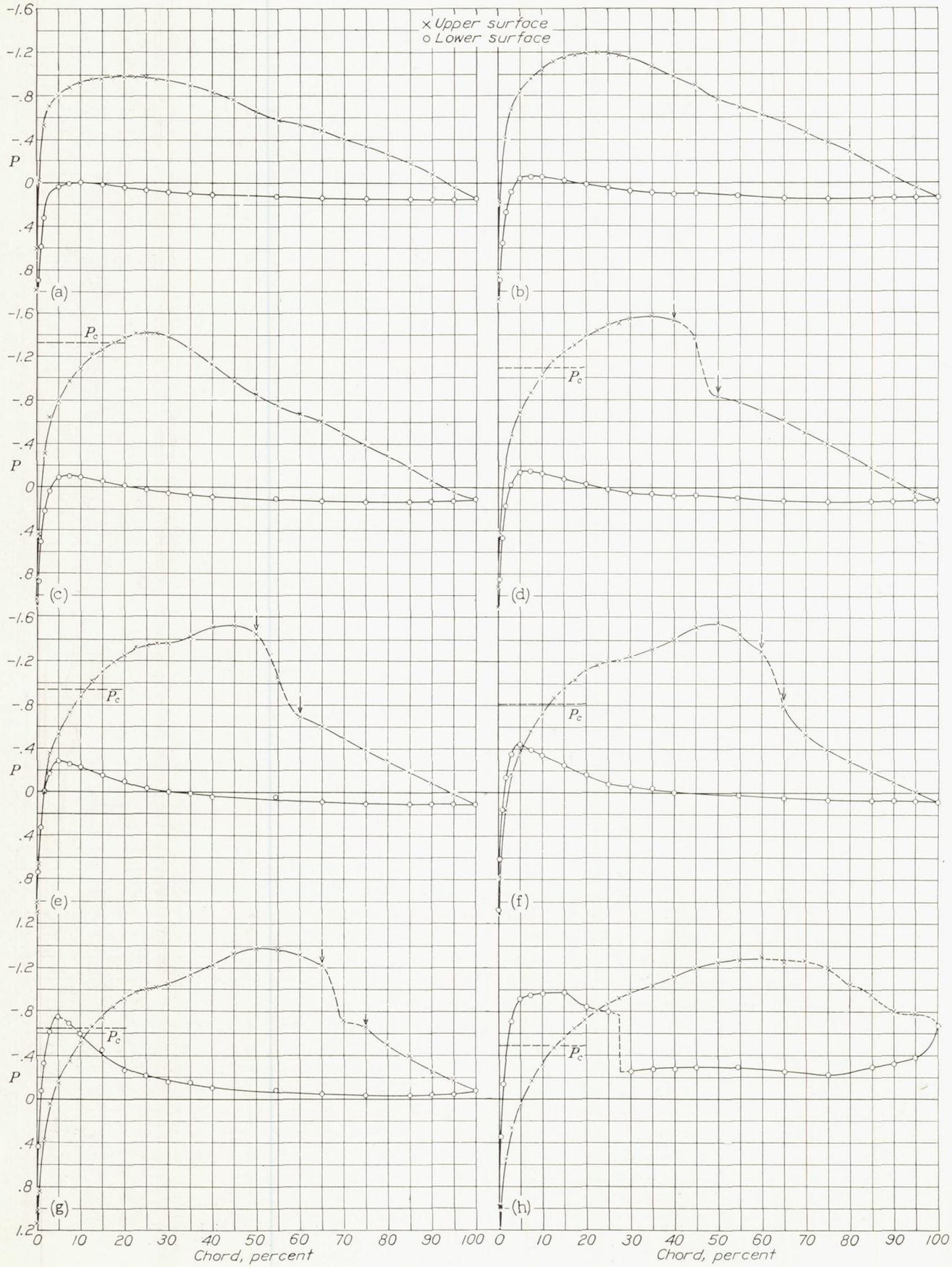

(a) $M=0.191$; test 24-26.
(b) $M=0.512$; test 24-27.
(c) $M=0.596$; test 24-12.
(d) $M=0.640$; test 24-27.
(e) $M=0.664$; test 24-12.
(f) $M=0.690$; test 24-12.
(g) $M=0.735$; test 24-12.
(h) $M=0.782$; test 24-27.

FIGURE 5.—Pressure distribution for the N. A. C. A. 4412 airfoil. $\alpha=1°52.5'$.

(a) $M=0.668$.

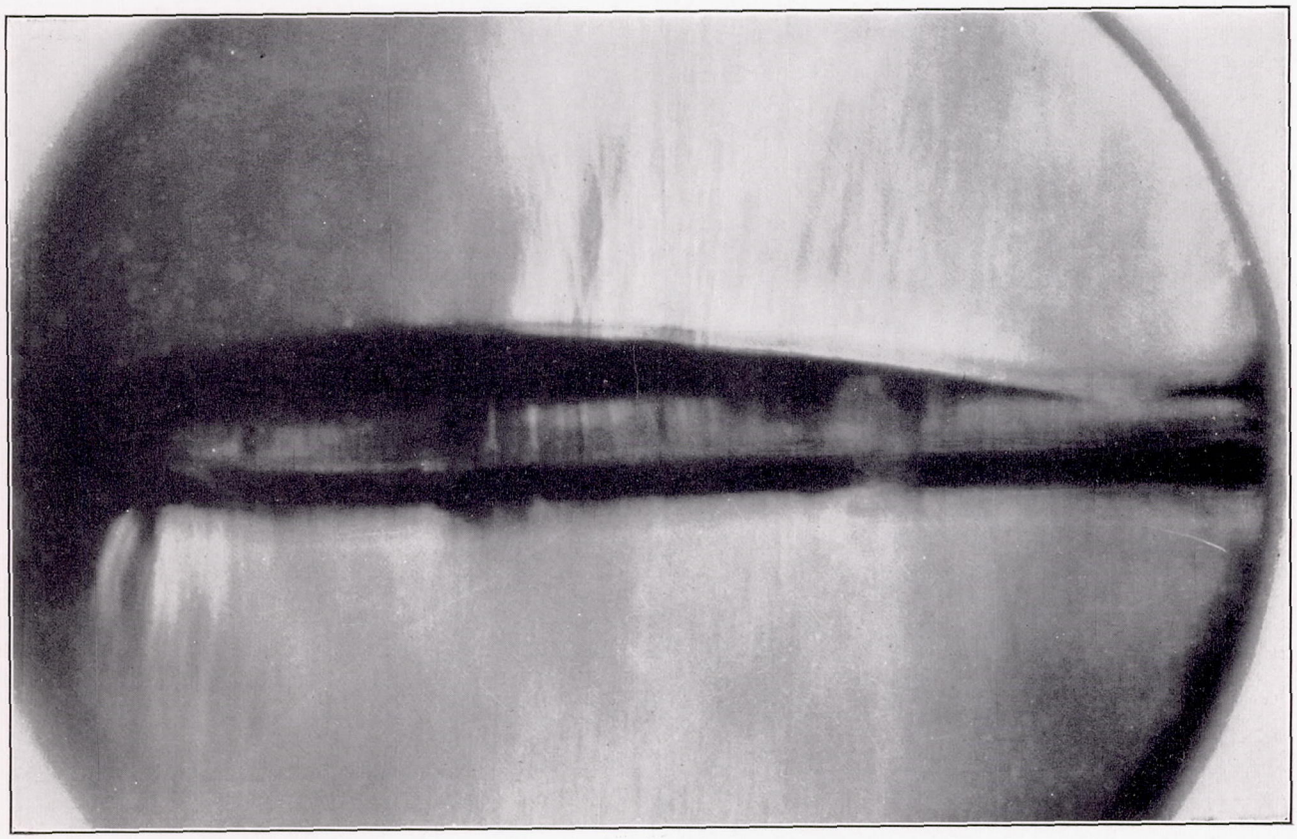

(b) $M=0.696$.

FIGURE 6.—Schlieren photographs of flow for the N. A. C. A. 4412 airfoil. $\alpha=-2°$.

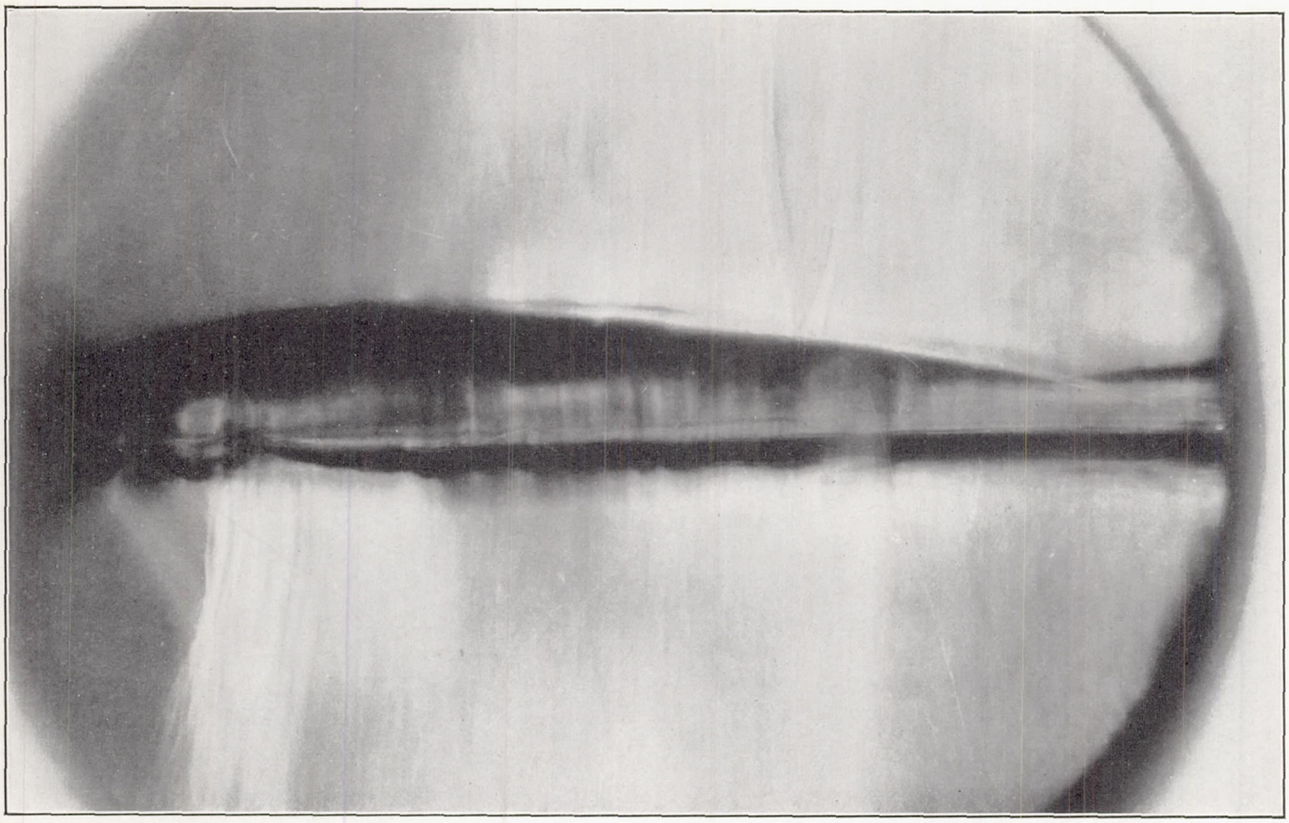

(c) $M=0.726$.

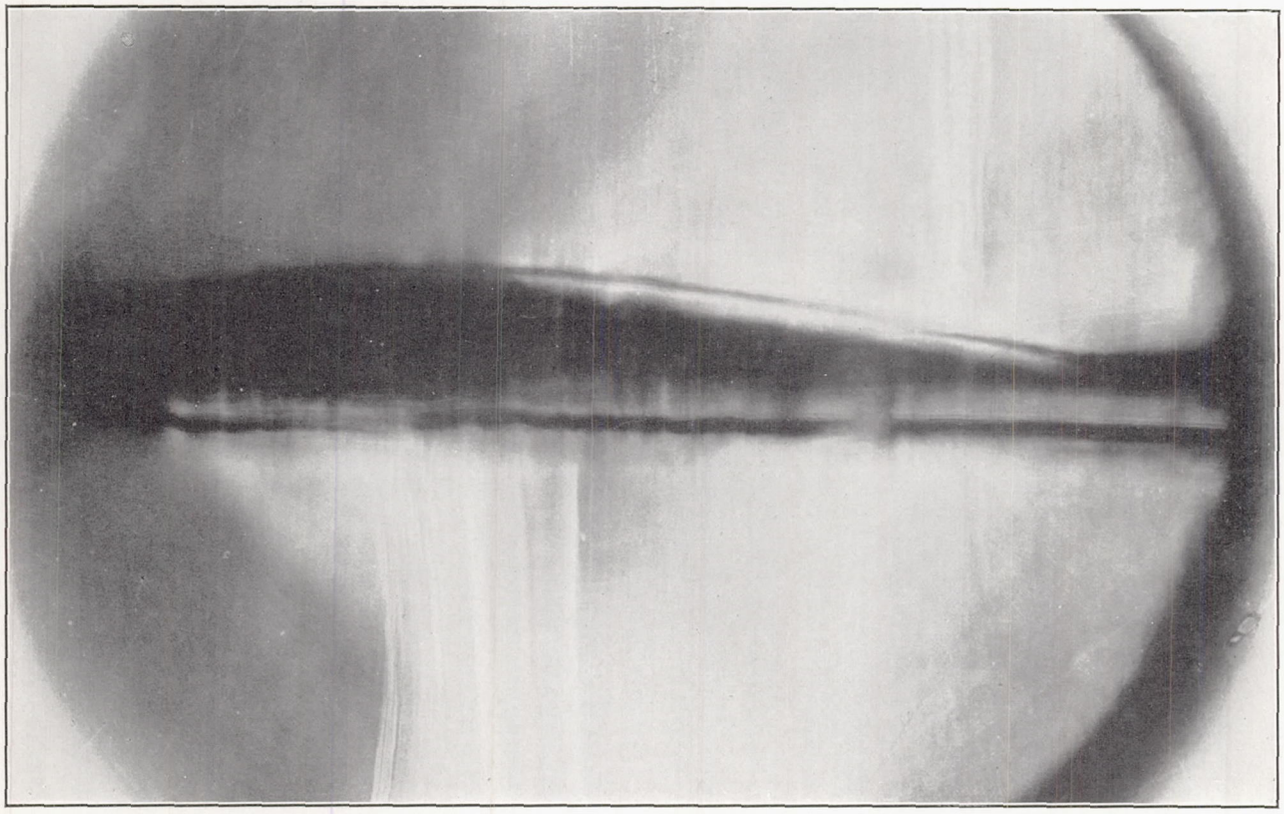

(d) $M=0756$..

FIGURE 6.—Schlieren photographs of flow for the N. A. C. A. 4412 airfoil. $\alpha=-2°$—Continued.

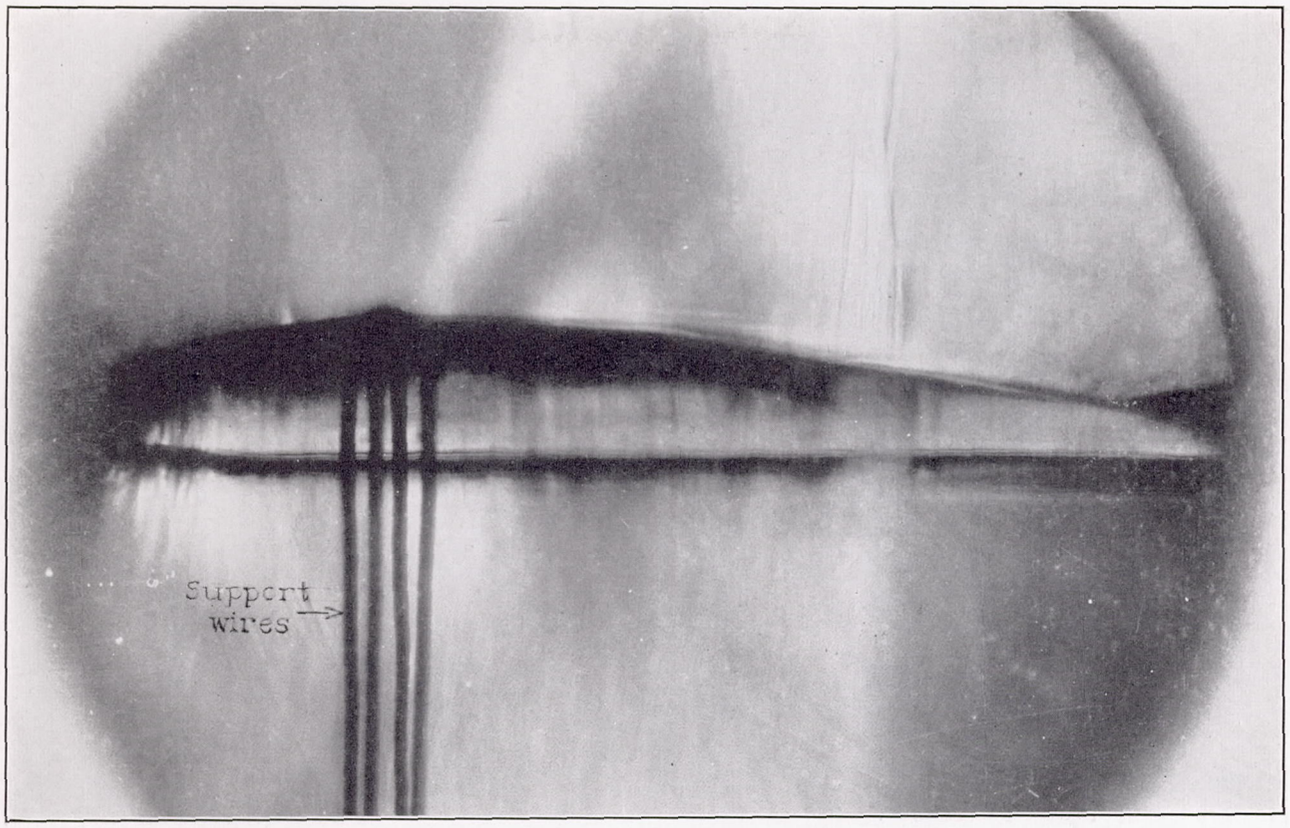

FIGURE 7.—Schlieren photograph of flow for the N. A. C. A. 4412 airfoil. $\alpha=-0°15'$; $M=0.717$.

DISCUSSION

Examination of the pressure-distribution diagrams and the flow photographs (figs. 3 to 8) will give a general indication of the effect of compressibility and an illustration of the nature of the flow changes that occur. At low speeds, the shape of the pressure-distribution diagrams is in agreement with the results of previous low-speed tests. As the speeds are increased, however, the area of the diagrams is increased as a result of the increases in the value of the local pressure coefficient. This change continues without appreciable modification of the general flow pattern until speeds in the field of flow equal or exceed the local speed of sound. When this condition occurs, there is a marked change in the type of flow.

The important characteristic of the flow now established is illustrated by figures 6, 7, and 8. A disturbance is formed as indicated by the sharp lines that project outward from the airfoil approximately perpendicularly to the airfoil surface. Correlation of the photographs and the pressure-distribution diagrams show that the location of the disturbance on the airfoil surface corresponds to the location of the discontinuity in the diagrams.

The dotted line on the diagrams shows the value of the pressure coefficient corresponding to the attainment of the local speed of sound. When values of the local pressure coefficient rise above the value corresponding to the local speed of sound, examination of the diagrams and the flow photographs indicates that a compression shock is formed which, with a further increase of speed, becomes more intense and moves back along the airfoil, ultimately reaching the trailing edge. Other data (reference 1) show that, when the trailing edge is reached, further increases in speed add considerable downstream slope to the disturbance.

Previous studies of compressibility effects have been based on force-test data; in order to correlate these data with the results of the present investigation, force-test data have been included in figures 9 and 10. A strict comparison is not possible because of previously explained differences in tunnel-wall effects for the force and the pressure-distribution tests. Changes due to compressibility, however, are comparable and it is apparent from examination of the figures that the results of the force tests and the integrated data obtained from the pressure-distribution tests are in excellent agreement regarding the effects of compressibility. As the speed is increased, the lift at first increases, the increase becoming greater until finally a speed is reached at which there is a sudden loss of lift. The rate of increase of lift is approximately the same for both the pressure-distribution and the force-test results, and the critical

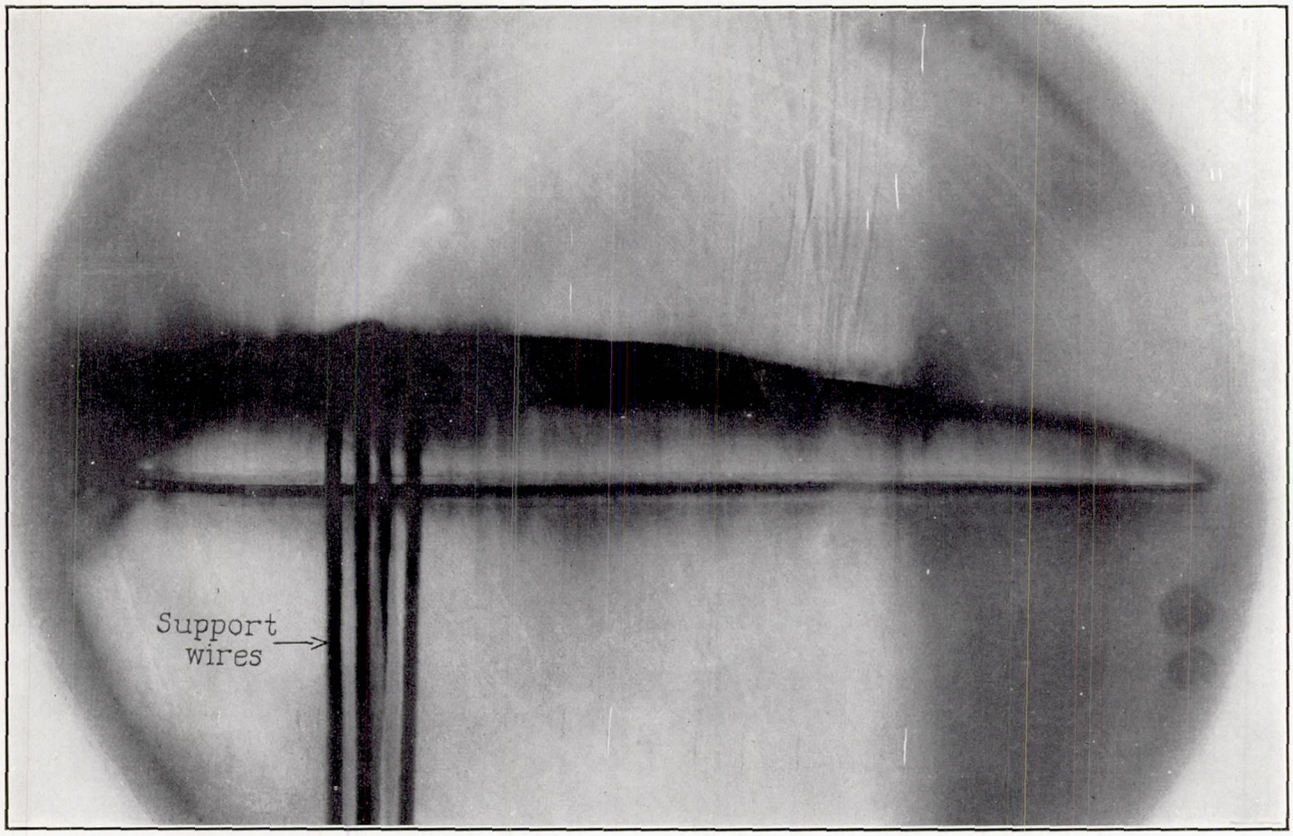

(a) $M=0.690$.

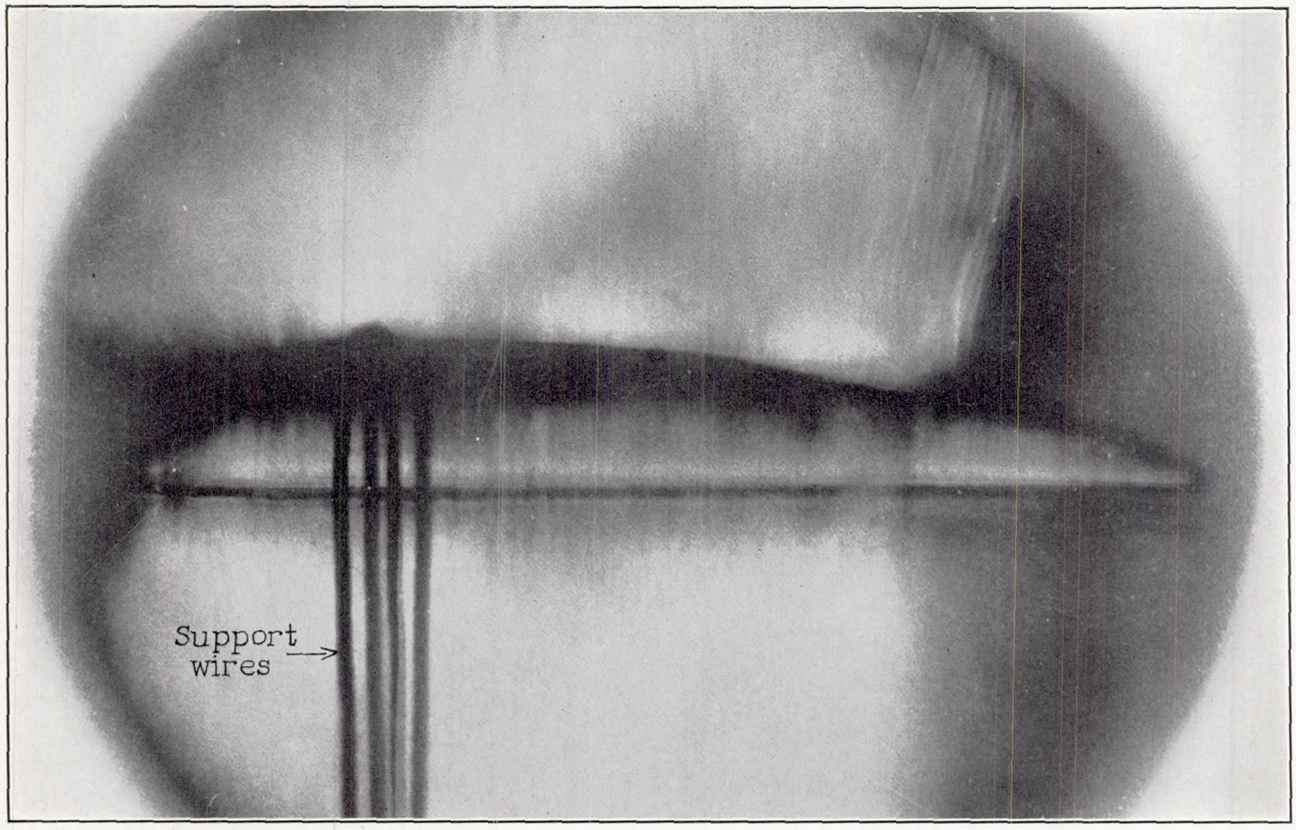

(b) $M=0.735$.

FIGURE 8.—Schlieren photographs of flow for the N. A. C. A. 4412 airfoil. $\alpha=1°52.5'$.

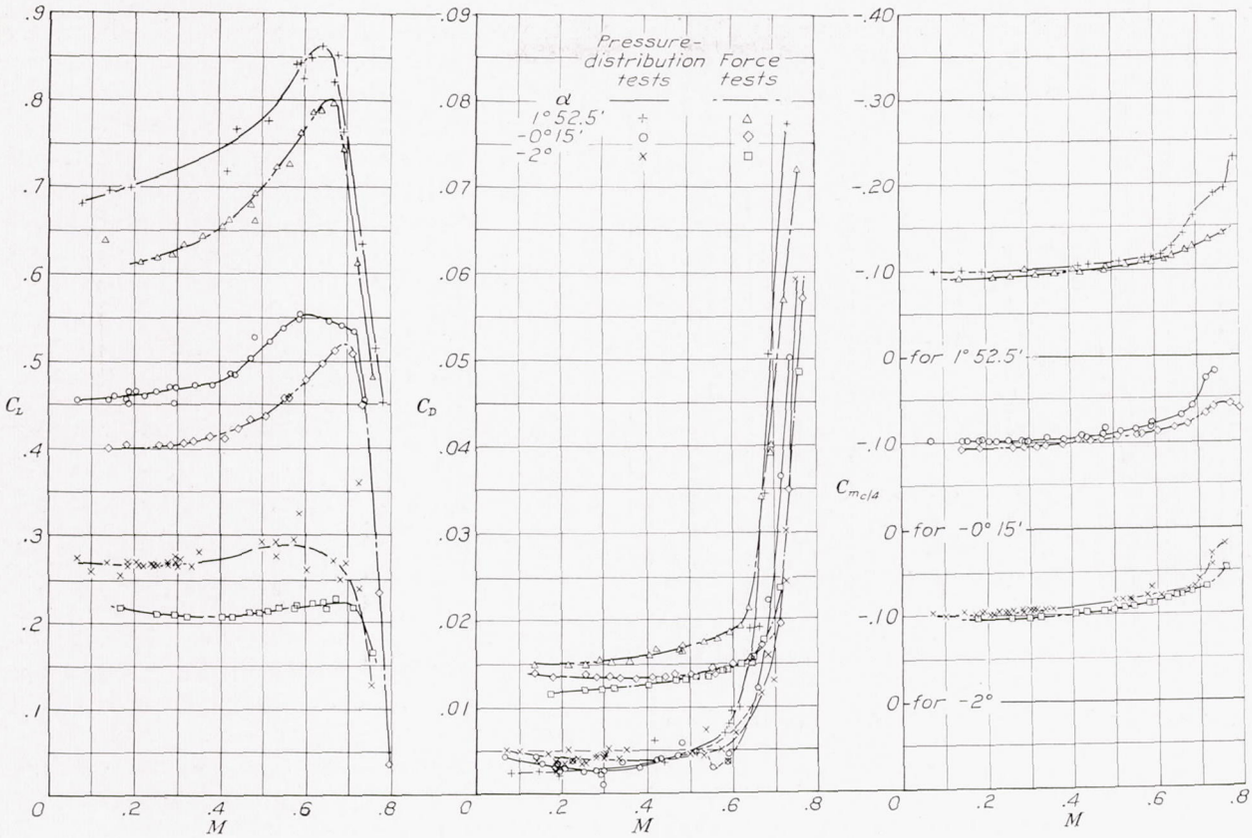

FIGURE 9.—Airfoil characteristics from the integrated pressure measurements and force-test data.

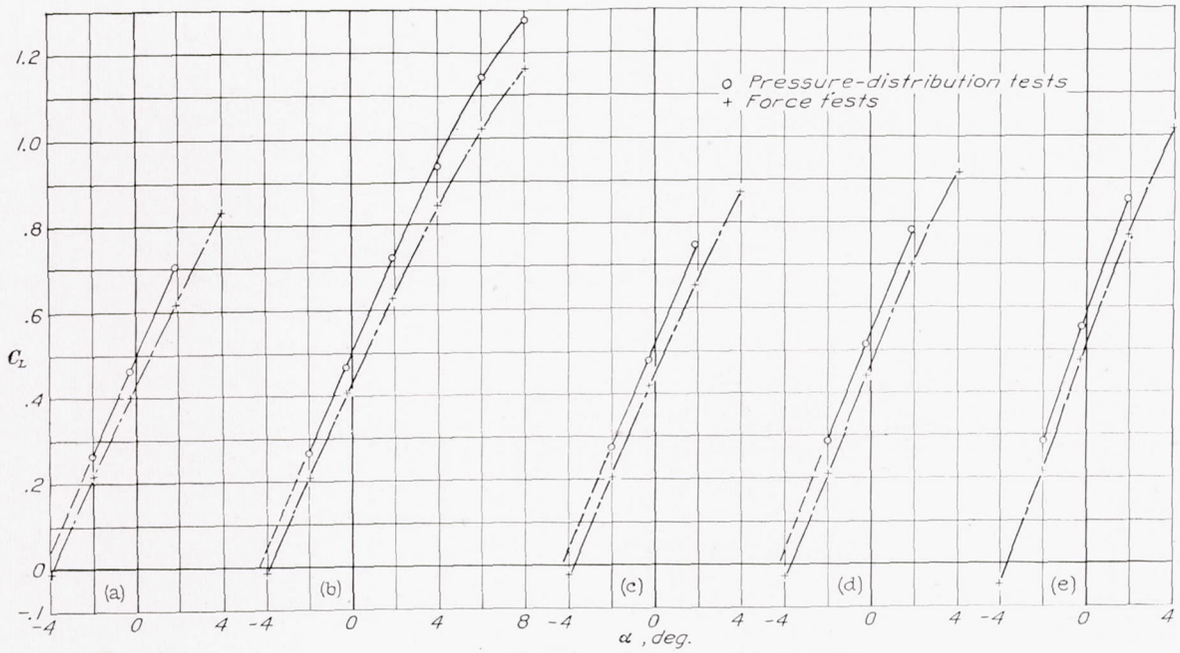

(a) M=0.2. (b) M=0.3. (c) M=0.4. (d) M=0.5. (e) M=0.6.

FIGURE 10.—Lift curves for the N. A. C. A. 4412 airfoil at several values of the compressibility index M.

speed for equal lift coefficients is in approximate agreement. Examination of the drag data illustrates relatively little change in drag until the critical speed is reached, when there is a rapid rise in the drag coefficient. It should be remembered, however, that the pressure-distribution results give only the pressure drag for approximately two-dimensional flow, whereas the force-test data include the friction drag and some induced drag due to tunnel-wall effects.

The effects of compressibility on the pitching-moment coefficient (fig. 9) are also in good agreement. As the speed is increased, there is first a gradual increase in the diving moment until the critical speed is reached, when the moment undergoes large and rapid increases.

Correlation of these data with the pressure-distribution diagrams and the flow photographs (figs. 3 to 8) shows that the critical speed is approximately the stream velocity for which the local speed of sound is attained at some point over the airfoil surface. The rise in drag and the loss in lift are therefore associated with the flow change that occurs when the compression shock is formed.

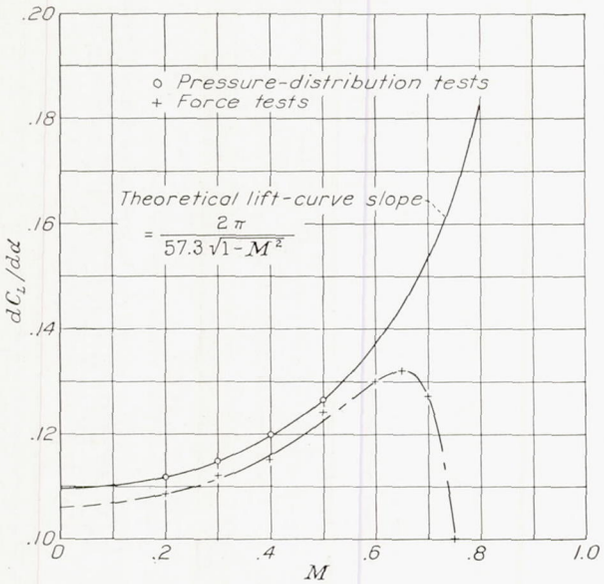

FIGURE 11.—Variation of lift-curve slope for the N. A. C. A. 4412 airfoil with the compressibility index M.

The data, in general, show that two types of flow occur. The first type is a flow similar to the usual low-speed type but changing progressively and uniformly in such a way as to give rise to increasing pressure coefficients, which type of flow exists for speeds up to the critical; that is, a flow with speeds nowhere exceeding the local speed of sound. The second type is a flow with compression shock in which speeds both above and below sound speed occur.

COMPRESSIBILITY EFFECTS IN THE SUBSONIC REGION

Glauert and Ackeret (references 7 and 8) have studied, theoretically, the effect of compressibility in a potential flow and, although their methods of analysis differed, both arrived at the same result. They found that the lift for a given angle, or the lift-curve slope, was increased by the amount $1/\sqrt{1-M^2}$. The theoretical result is in agreement with these experiments, as shown in figure 11. Ordinarily, the agreement is not so good as shown by this particular airfoil but the theoretical variation does, in general, correlate the differences in lift between high and low speeds provided, of course, that the critical speed is not exceeded.

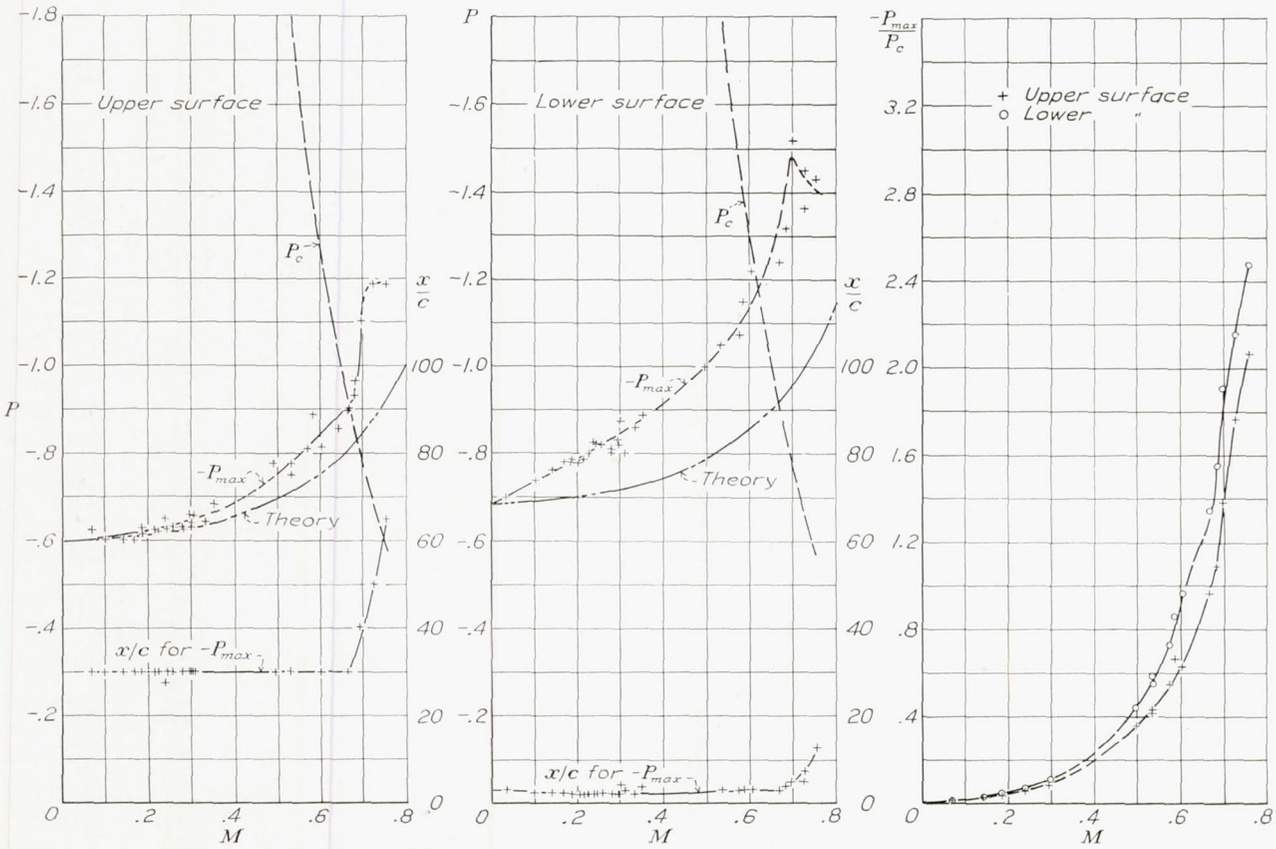

FIGURE 12.—Effect of compressibility on the maximum negative pressure coefficient for the N. A. C. A. 4412 airfoil. $\alpha=-2°$.

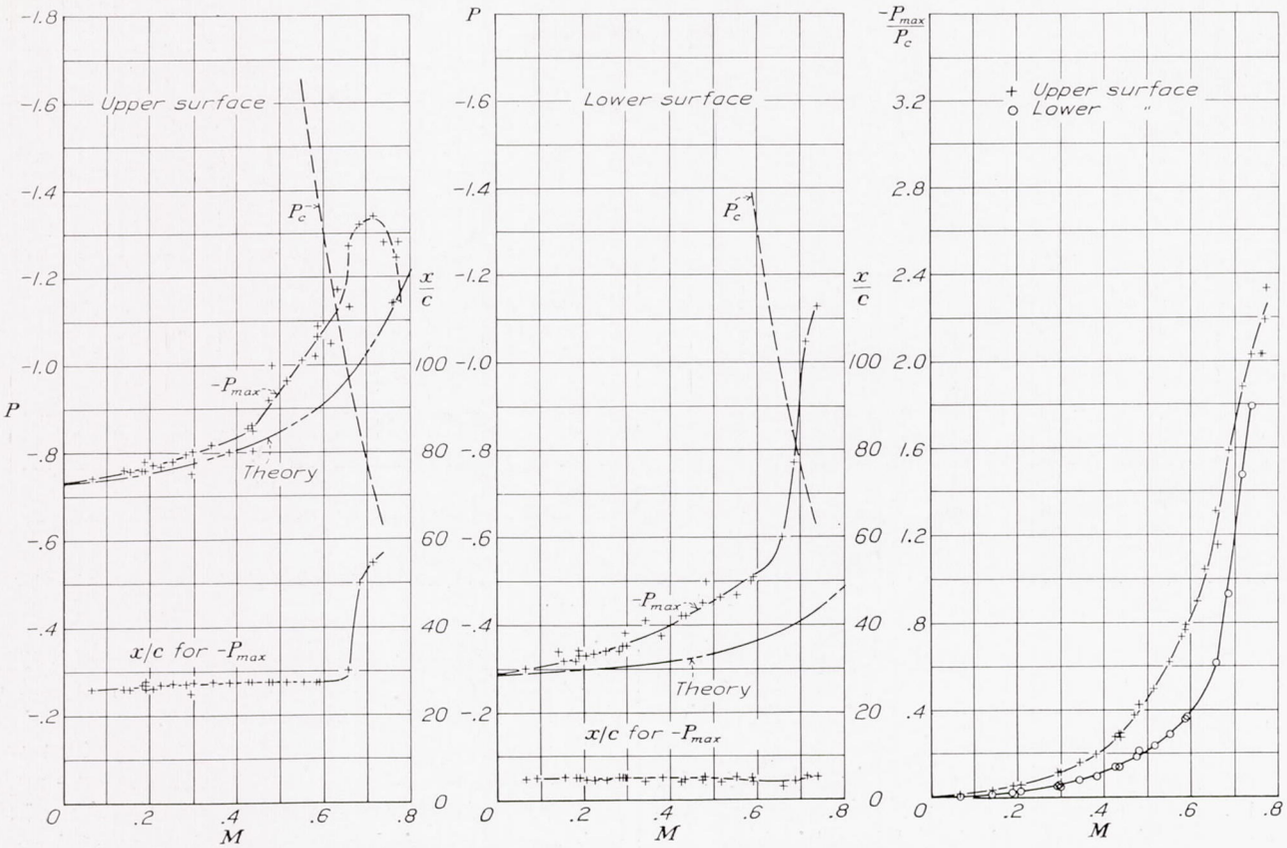

FIGURE 13.—Effect of compressibility on the maximum negative pressure coefficient for the N. A. C. A. 4412 airfoil. $\alpha=-0°15'$.

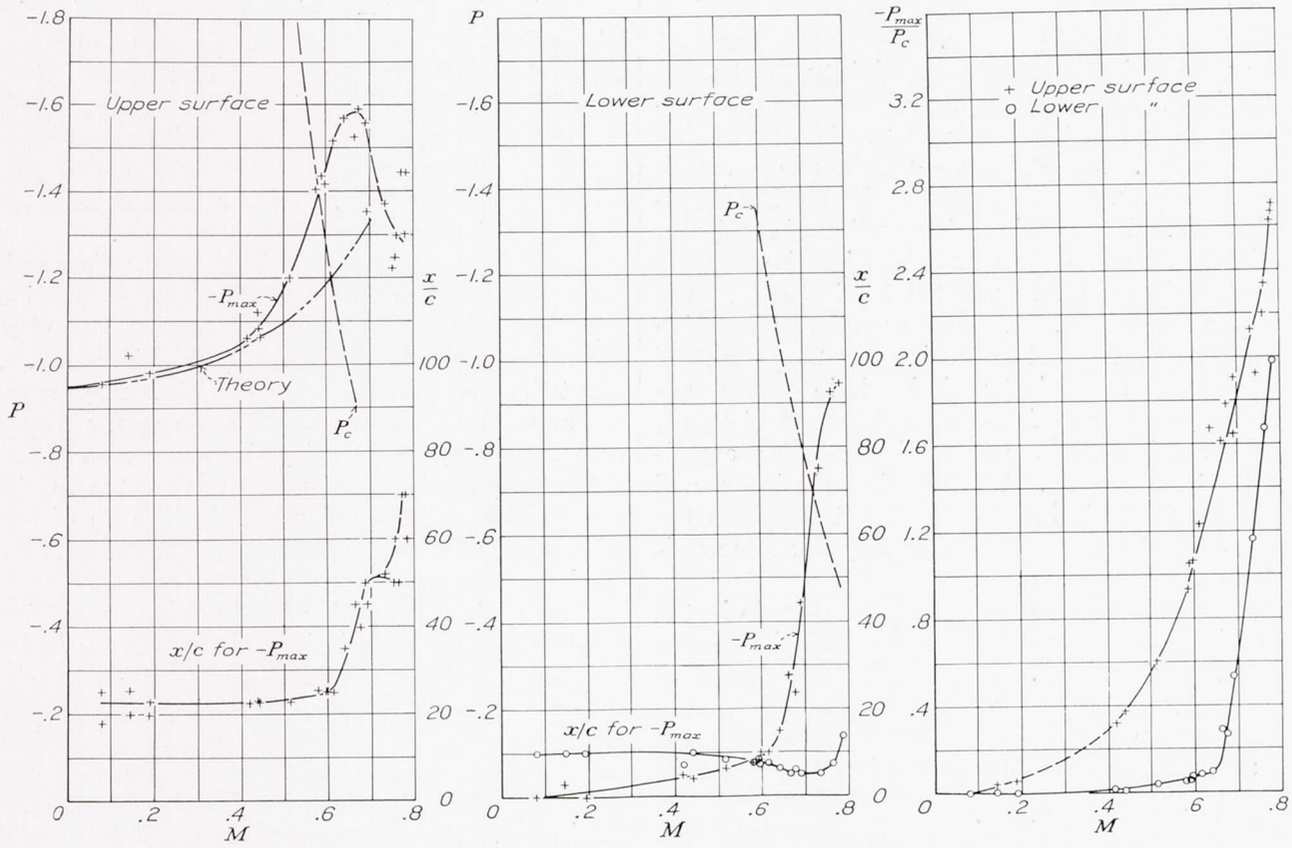

FIGURE 14.—Effect of compressibility on the maximum negative pressure coefficient for the N. A. C. A. 4412 airfoil. $\alpha=1°52.5'$.

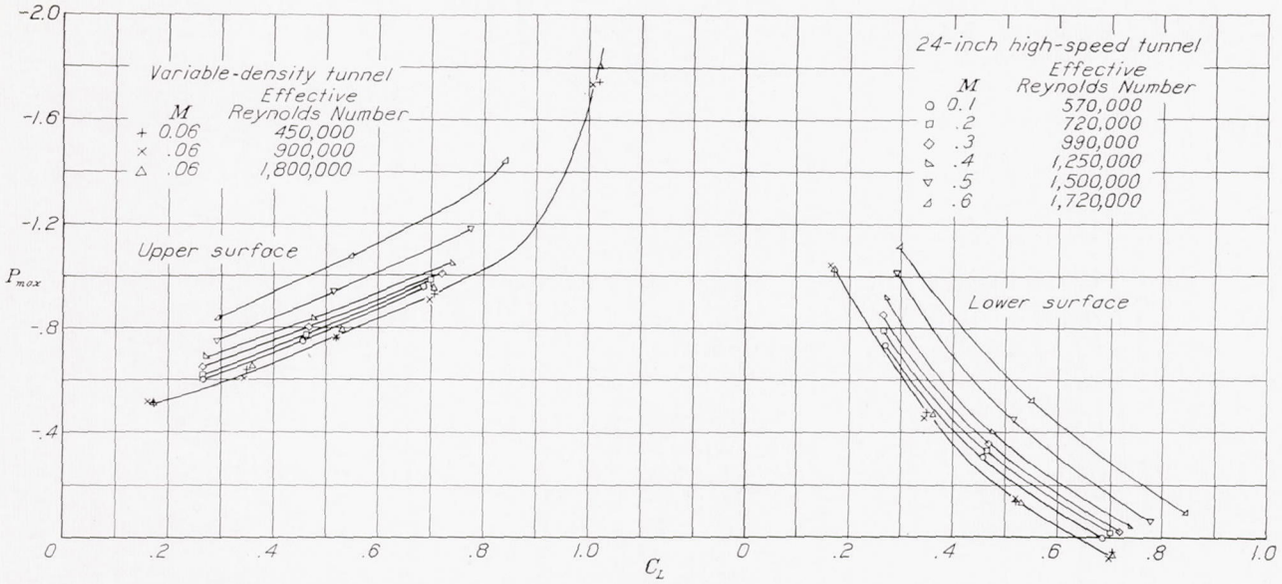

FIGURE 15.—Variation of maximum negative pressure coefficient with lift coefficient as affected by compressibility index M and effective Reynolds Number for the N. A. C. A. 4412 airfoil.

Ackeret concluded from his analysis that the local induced-pressure differences, as well as the lift, would likewise be increased; a comparison of the theoretical result with the maximum negative pressures obtained on the surface of the airfoil is given in figures 12, 13, and 14. The location of the maximum negative-pressure coefficient, the variation of the critical-pressure coefficient, and the ratio of the maximum negative-pressure coefficient to the critical-pressure coefficient are also shown on the figures. The data show that theory underestimates the compressibility effect when the maximum negative pressure occurs near the leading edge and when the speeds exceed four-tenths the speed of sound. At $-2°$ and $-0°15'$ angle of attack (figs. 12 and 13), the disagreement for the lower surface is large. The location of the point of maximum negative pressure for these two conditions is less than 5 percent of the chord from the leading edge, as is shown by the figures. When the maximum negative pressures occur back of approximately 20 percent of the chord, the theoretical variation is in good agreement for speeds up to four-tenths the speed of sound, but above this speed the theoretical and the experimental results diverge. The practical significance of this disagreement is important in that it affects the accuracy of estimates of the critical speed; these estimates will be discussed later.

The probable reasons for the discrepancy lie in the assumptions and the approximations made in the development of the theory. The most important assumption affecting the accuracy of the theory concerns the induced velocities, which are assumed to be negligibly small; and, further, in order to obtain a usable result, the speed of sound is assumed constant throughout the flow field. The approximation for the speed of sound can, in fact, be shown to be equivalent to an assumption of zero as the value of the induced velocity. Disagreement with the theory may thus be expected when the induced velocities, as is usual, depart considerably from negligibly small values.

The development of a rigorous theory that would enable the computation of the actual pressures appears improbable for practical use, but examination of theoretical results available (references 5, 9, and 10) appears to indicate that, at least near the leading edge, the approximation $1/\sqrt{1-M^2}$ is not completely descriptive of the changes that may occur. It may be possible to arrive theoretically at a result that agrees with the experiments. The theoretical treatment is exceedingly complicated and an accurate result, if present methods are used, can be arrived at only by a method of successive approximations. The problem should, nevertheless, be further examined theoretically.

Apart from the discrepancies thus far discussed between the theory and the experiments, theory provides no clue regarding the limits within which the application of the theory may be expected to yield fair results. Any effect that Reynolds Number variations may have and the upper limit of speed to which the theory is applicable must of necessity be determined from other sources.

The effect of Reynolds Number on the maximum negative pressures obtained appears to be of no importance within the range of these experiments. Figure 15 shows the results of tests made of the same model at low speeds in the variable-density wind tunnel for the Reynolds Number variation covering the data herein presented (reference 11). The measured maximum negative-pressure coefficients for the upper and the lower surfaces are plotted against lift coefficient in figure 15. It is apparent from the low-speed results ($M=0.06$) that the Reynolds Number effects are insignificant. The marked progressive displacement of the curves for the higher speeds then indicates that the pressure coefficients are far more seriously affected by

compressibility than by Reynolds Number within the range of these tests. It is important to note, therefore, that data taken at high Reynolds Numbers obtained by increasing the speed must be corrected for compressibility if they are to be applied at equal Reynolds Numbers but at lower speeds.

The upper limit of the speed range to which the theoretical allowance for compressibility effects may be applied with fair results can logically be assumed to be the speed at which the potential flow postulated by the theory fails as a result of the formation of a compression shock. In itself, however, the theory indicates no definite limit other than the speed of sound; therefore other means for studying the condition must be used. This problem will be further discussed in connection with the derivation of methods for estimating the critical speed.

COMPRESSIBILITY EFFECTS IN THE SUPERCRITICAL REGION

The phenomena in the supercritical region, that is, for speeds above that at which the compressibility burble occurs, are entirely unrelated to those just discussed. The discontinuities in the pressure-distribution diagrams and the corresponding schlieren photographs indicate that compression shock occurs when the maximum velocity over a portion of the airfoil exceeds the local speed of sound. With further increase in stream velocity, the local velocities over the forward portion of the airfoil continue to increase, greatly exceeding the local speed of sound; the discontinuity, or compression shock, moves rearward along the airfoil, ultimately reaching the trailing edge. With further increase of the stream velocity, other tests (reference 1) have shown that the shock remains at or near the trailing edge but with considerable downstream slope, the slope increasing with speed. The significant characteristic of the flow in the supercritical region appears to be the existence of supersonic speeds over a portion of the airfoil and, of course, the compression shock that occurs at the downstream boundary of the supersonic speed region.

The occurrence of the compression shock can be visualized from elementary considerations. It has been shown that the speed of sound is the normal rate of pressure propagation; therefore the high-pressure low-speed field existing at the rear of the airfoil can affect the flow in the supersonic region only at the boundary. Within the supersonic field, the velocity and the pressure at any point are thus uninfluenced by conditions in the low-speed high-pressure region at the rear of the airfoil; but ultimately the low-pressure air must be compressed to return to equilibrium with the air stream back of the model. Compression of the supersonic air in smooth normal fashion requires, as nozzle studies have indicated, a contraction of the stream. The stream boundary formed by the airfoil, however, is the reverse, forming effectively an expansion; and, in supersonic flow, this expansion leads to further increases in speed with still lower pressures. As the low-pressure air cannot pass off into the high-pressure region without setting up the obvious impossibility of tension, some unusual type of flow must occur.

Imagine, momentarily, that the low-pressure air of high kinetic energy meets the high-pressure region and that equilibrium is established through interchange of the kinetic energy of the molecules of the low-pressure and the high-pressure air. If the layer through which equilibrium was brought about were infinitely thin, then the obvious impossibility of regions of tension in the air is circumvented. In the energy interchange, the pressure of the air of supersonic speed would be increased to values that would permit normal compression over the rear part of the airfoil, and these values would generally exceed the pressure corresponding to the local speed of sound. Following the layer or compression shock, subsonic speeds would occur and compression over the remaining portion of the airfoil would take place in the normal manner. Within the compression shock, however, a considerable amount of kinetic energy would be dissipated in the energy interchange because of the internal friction, or viscosity, of the air. The energy dissipated by the internal friction, or viscosity, would be converted into heat, thereby becoming unavailable to the flow, and would appear in the flow as decreased total pressure or increased drag on the model.

The movement of the shock front with increasing speed is not well understood, but it is possible to reason why the shock front should move rearward with increasing speed. If the influence of any local pressure disturbance is considered to be transmitted in all directions at the normal speed of sound, at any and all time intervals a pressure disturbance at the trailing edge will proceed from the trailing edge at the local speed of sound. The forward-moving portion of the disturbance, however, travels at a speed that decreases because of the increasing local velocity of flow at points close to the airfoil surface. Finally, the forward-moving portion of the disturbance is stopped at a point where its local velocity equals the local stream velocity; a sharp front thus results as the continuous disturbance from the trailing edge piles up. In the shock front, however, the local speed of sound is increased over the normal stream value owing to the intensity of the disturbance that has now been formed and because of the increased speed of sound resulting from the temperature or heat increase at the shock. The velocity at the front thus exceeds the normal speed of sound in the stream. Ultimately, however, an equilibrium is reached at some point on the airfoil where the supersonic speed over the forward portion is equal to the local speed of propagation of the disturbance. At this point, then, the transverse compression shock is stationary. Now, with increasing stream velocity,

the local velocities in front of the shock are increased and the shock front therefore tends to be swept farther back to a new equilibrium position. The intensity of the shock tends to become somewhat more severe, as indicated by previous discussion; but it appears from the experimental data that the increase in local speed of sound at the shock front is not so rapid as the increase in the local velocity of flow over the forward portion of the airfoil with increase of stream velocity.

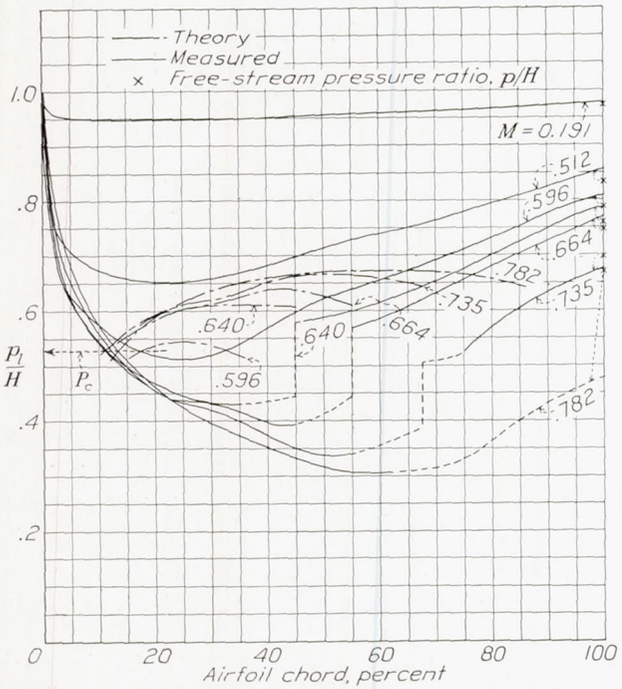

FIGURE 16.—Comparison of theoretical pressure after shock and pressure measurements. N. A. C. A. 4412 airfoil. $\alpha=1°52.5'$.

If this condition is assumed, then, the shock front must move to the rear with an increase in speed.

Similar phenomena have been observed in nozzles operating with excessive back pressure (reference 12). Prandtl and others have examined the phenomena and find that considerable energy is lost in the compression shock. Briefly, the high-speed air at the compression shock loses a large amount of kinetic energy, only a part of which is recovered as pressure; and the remaining energy, becoming unavailable to the flow, appears as heat. From studies of the phenomena occurring in a nozzle, formulas for calculating the increase in pressure due to the compression shock have been derived. These methods were first applied to an airfoil in reference 2. From the pressure formula of reference 2,

$$\frac{p_2}{p_1}=\frac{2\gamma}{\gamma-1}\left[\frac{2}{\gamma+1}\left(\frac{p_1}{H}\right)^{\frac{1-\gamma}{\gamma}}-1\right]+1$$

Figure 16 has been prepared to compare the results of the calculated and the measured pressures behind the shock. The measured data are for the airfoil upper surface for an angle of attack of 1° 52.5′, and the data are plotted as ratios of the local absolute pressure to the total pressure or the pressure at the stagnation point of the airfoil.

Because the theory does not give a clear indication of the point at which the compression shock occurs, the theoretical curves of figure 16 were determined by assuming that shock may occur for any pressure in the supersonic-flow region of the airfoil and then computing the corresponding pressure after the shock. The difference between the theoretical and the experimental curves at any point along the chord thus shows the theoretical increment in pressure if shock had occurred at that point on the airfoil. The location of the shock is shown by the experimental results and therefore, at this location, the measured and the theoretical pressure changes in the actual shock can be compared. It is apparent that the calculated pressure increases far exceed the measured values.

There are several reasons for the discrepancy. Fundamentally, however, the theory of simple shock assumes compression in an infinitely thin layer from the pressure corresponding to the maximum flow velocity in front of the shock to the final pressure after the shock. Actually, the compression does not take place in this manner. Some of the diagrams indicate that some small compression occurs smoothly, and probably without material energy loss, just before the shock; likewise, behind the shock, a similar condition appears. Further, the shock does not occur in an infinitely thin layer. These effects would tend to lessen the intensity of the shock by allowing less deceleration of the more rapidly moving molecules in the supersonic region. In the computation of the theoretical pressure increments, the one-dimensional-flow equations are used, which are based on the assumption that the flow passes through the shock perpendicular to the wave front; the possibility of separation and the effect that it may have on the direction of the flow are not considered. Separation is extremely likely, because the shock is, in effect, a large adverse-pressure gradient. Considerable further experimentation appears to be necessary.

The magnitude of the kinetic-energy loss in the shock for all the data has been computed from the pressure-distribution data and the results are shown by the plotted points in figure 17. The abscissas have been taken as the ratio of the local pressure in front of the shock to the total pressure in front of the shock, rather than the compressibility index of the air stream M, to permit better correlation of all the data. Had the air stream M been chosen for the abscissas, the data for each angle of attack would have been displaced and no clear indication of the critical pressure at which the shock forms could have been obtained. The ordinates, the kinetic-energy-loss coefficients, represent the difference between the kinetic-energy change in the shock and the work done by the air in overcoming the pressure difference at the shock divided by the kinetic

energy in front of the shock. When no shock occurs, the value of the kinetic-energy-loss coefficient is zero.

Briefly, the formula is derived as follows:

$$K_{E.L.}=\frac{K.\ E._{loss}}{K.\ E._1}=\frac{\Delta K.\ E.-(\text{work done})}{K.\ E._1}$$

where $K_{E.L.}$ is the kinetic-energy-loss coefficient and $K.\ E._1$ is the kinetic energy in front of the shock. If it is assumed that

$$\rho_1 u_1=\rho_2 u_2$$

and

$$p_2-p_1=\rho_1 u_1(u_1-u_2)$$

where u is the local velocity of the air stream,

$$K_{E.L.}=\frac{\left(\frac{p_2}{p_1}\right)^2-1}{\left(\frac{2\gamma}{\gamma-1}\right)^2\left[\left(\frac{H}{p_1}\right)^{\frac{\gamma-1}{\gamma}}-1\right]^2}$$

In the computation of the values of $K_{E.L.}$ shown in figure 17, the pressures are taken from the pressure-distribution diagrams of figures 3 to 5. In general, the value of p_2 appears to be near the pressure corresponding to the local speed of sound in front of the shock. The values of p_1 and p_2 taken for the calculations are indicated by the arrows on the pressure-distribution diagrams.

The experimental data are consistent in regard to the amount of kinetic energy lost for any given pressure ratio but the actual loss is approximately half the theoretical value. The discrepancy arises for exactly the same reasons that the experimental and the theoretical pressure increments in the shock fail to agree. Theoretically, it is assumed that the shock is an infinitely thin layer and that all the compression occurs within the layer. The pressure diagrams show that the disturbed region is rather wide and indicate that the actual discontinuity is preceded and followed by regions of increasing pressure in which there is probably no loss. Very little is actually known of the flow in the disturbed region but the existence of a region of adiabatic compression immediately ahead of the shock, in particular, should be further investigated to determine the possibility of extending this region and thus of obtaining reduced shock intensity or a delayed compressibility burble.

The loss in total pressure caused by the shock on the upper surface of the airfoil is shown in figures 18 to 21. Figures 18 to 20 show the distribution of the loss and the pressure-distribution diagrams for the upper surface of the airfoil. No loss due to compression shock occurs until the stream velocity exceeds the local speed of sound. For even small speed increments above the critical, however, there are large increases in the total-pressure loss. The extent of the shock in a direction perpendicular to the chord in extreme cases (speeds at the trailing edge in excess of sound speed) is large and is approximately 130 percent of the chord. The shock thus extends about half the tunnel radius from the model. Near the model ends, therefore, there may be some tunnel-wall effect that may tend to intensify the shock locally. This effect, however, should not be of importance at the center section where these measurements were made.

Integrated values of the total-pressure loss due to the compression shock are a measure of the drag increments experienced by the airfoil. These values for all the angles of attack investigated are shown in figure 21

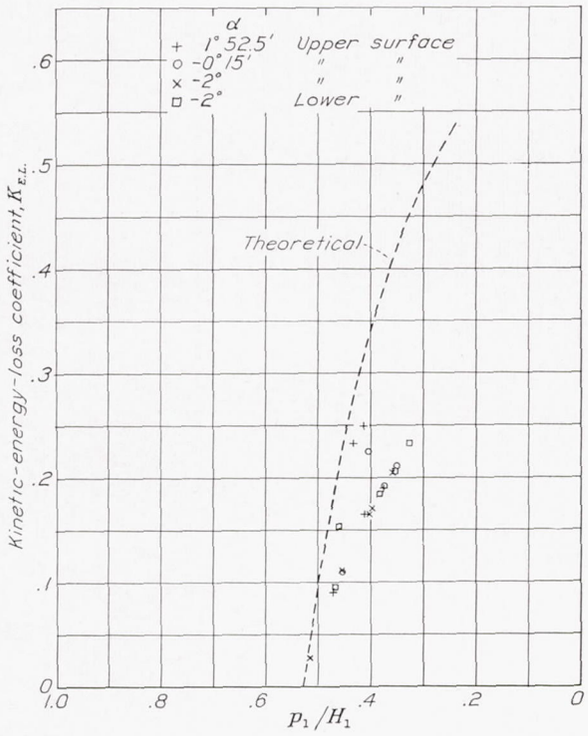

FIGURE 17.—Kinetic-energy-loss coefficient for the compression shock on the N. A. C. A. 4412 airfoil.

against the pressure ratio p_1/H and, though only qualitative as previously explained, the increase of the loss with decrease of pressure ratio p_1/H or increase of speed is consistent with the increase that might be expected from pressure-distribution and force-test data.

The theoretical total-pressure loss appears to be somewhat less than the values measured and integrated, which indicates a serious loss other than the direct shock loss. This possibility is further illustrated by the pressure change in the shock, indicated by the total-pressure measurements shown in figures 18 to 21. These pressure differences were obtained by assuming the total-pressure loss in the shock to be represented by the maximum value of the ratio $(H-H_2)/H$ outside the normal wake region. From the theoretical relation, the corresponding value of the pressure in front of the shock was determined and the corresponding pressure behind the shock was computed. The very large disagreement between the pressure changes thus shown and the measured values indicated by the pressure-distribution diagrams can hardly be accounted for by any of the previously discussed limitations of the theory. The results seem to indicate energy losses in addition to the

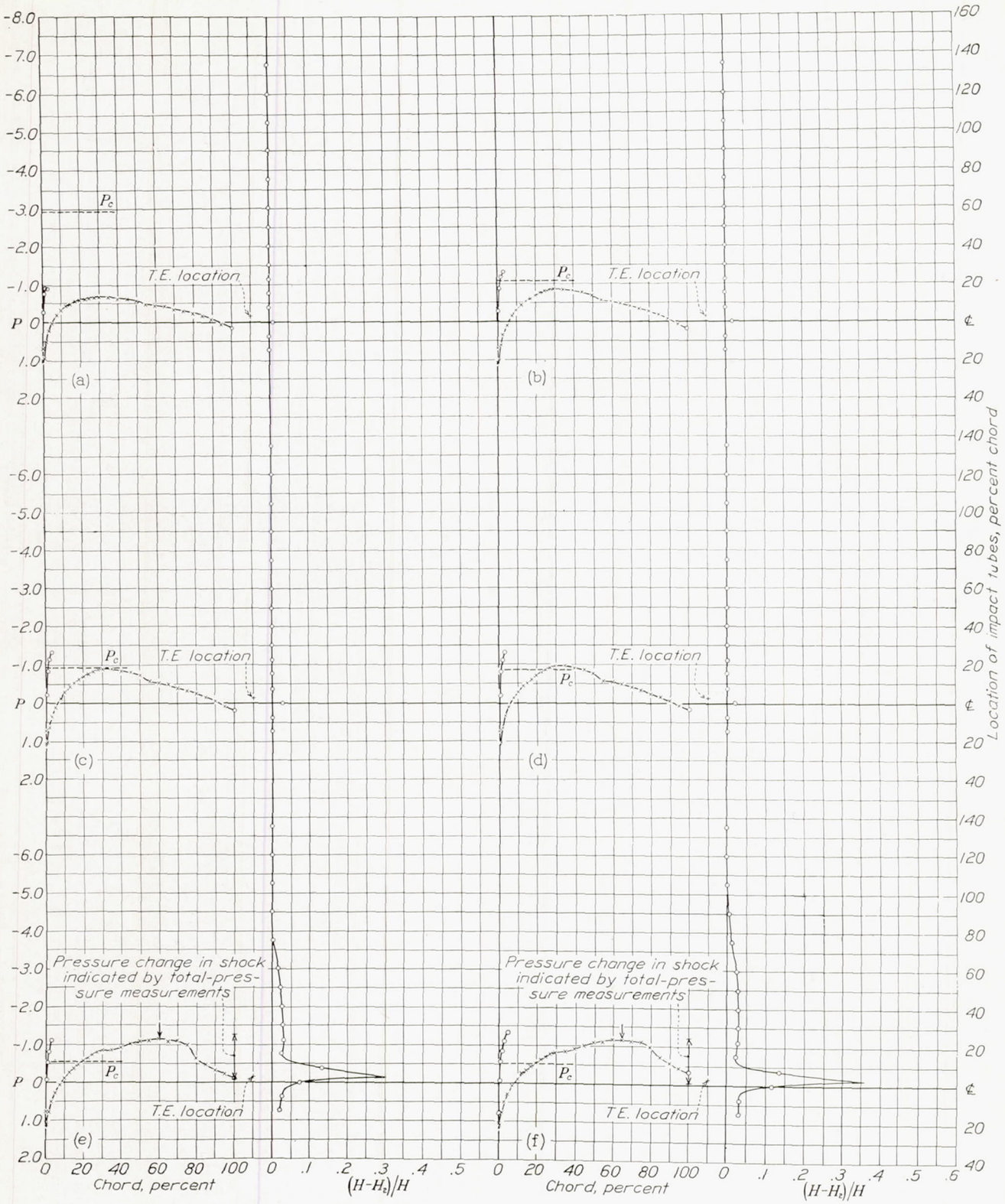

(a) $M=0.437$; test 24–27.
(b) $M=0.644$; test 24–27.
(c) $M=0.666$; test 24–27.
(d) $M=0.682$; test 24–27.
(e) $M=0.771$; test 24–27.
(f) $M=0.780$; test 24–27.

FIGURE 18.—Pressure distribution and compression shock total-pressure loss for the N. A. C. A. 4412 airfoil. $\alpha=-2°$.

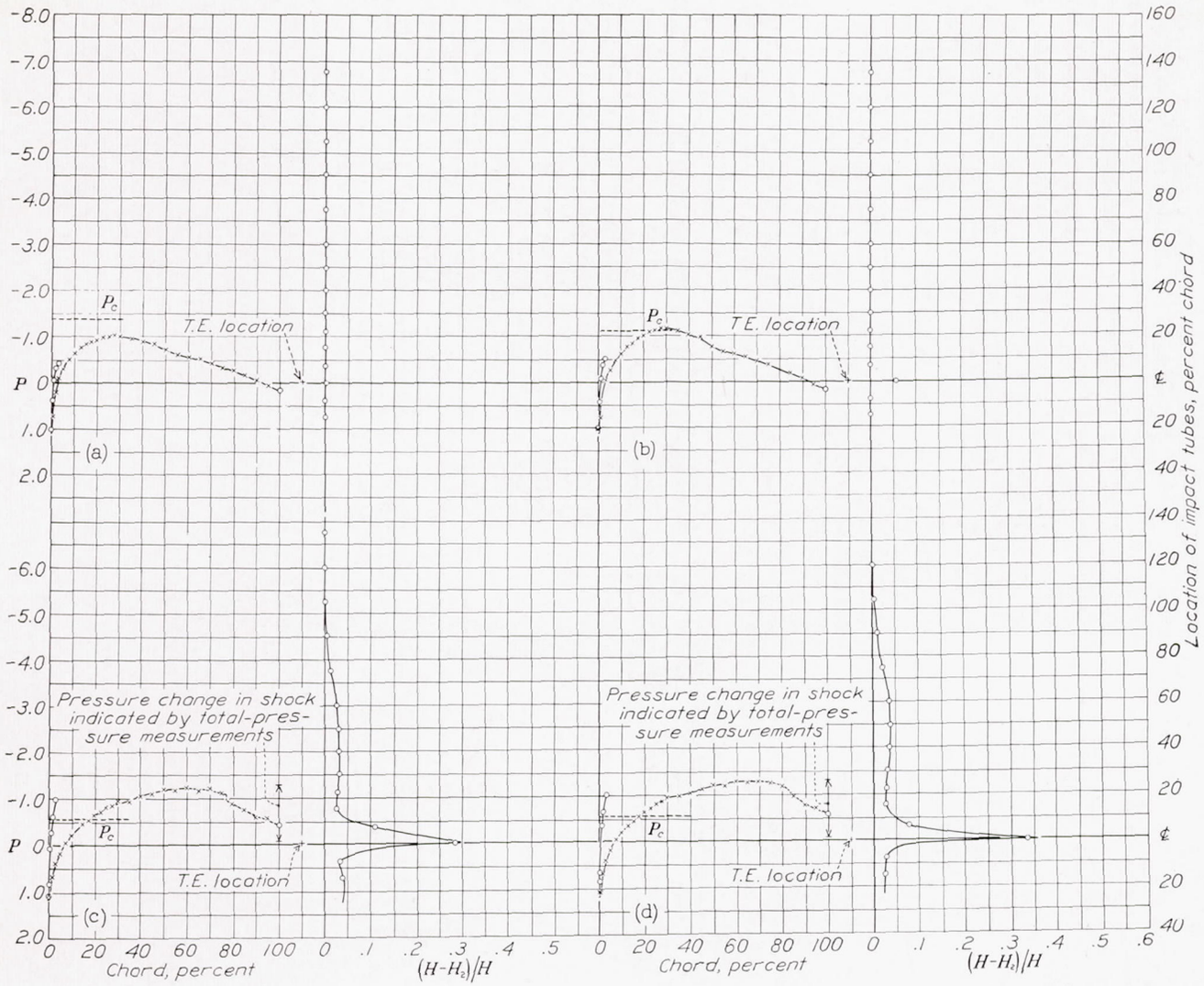

(a) $M=0.582$; test 24–27.
(b) $M=0.632$; test 24–27.
(c) $M=0.770$; test 24–27.
(d) $M=0.773$; test 24–27.

FIGURE 19.—Pressure distribution and compression shock total-pressure loss for the N. A. C. A. 4412 airfoil. $\alpha=-0°15'$.

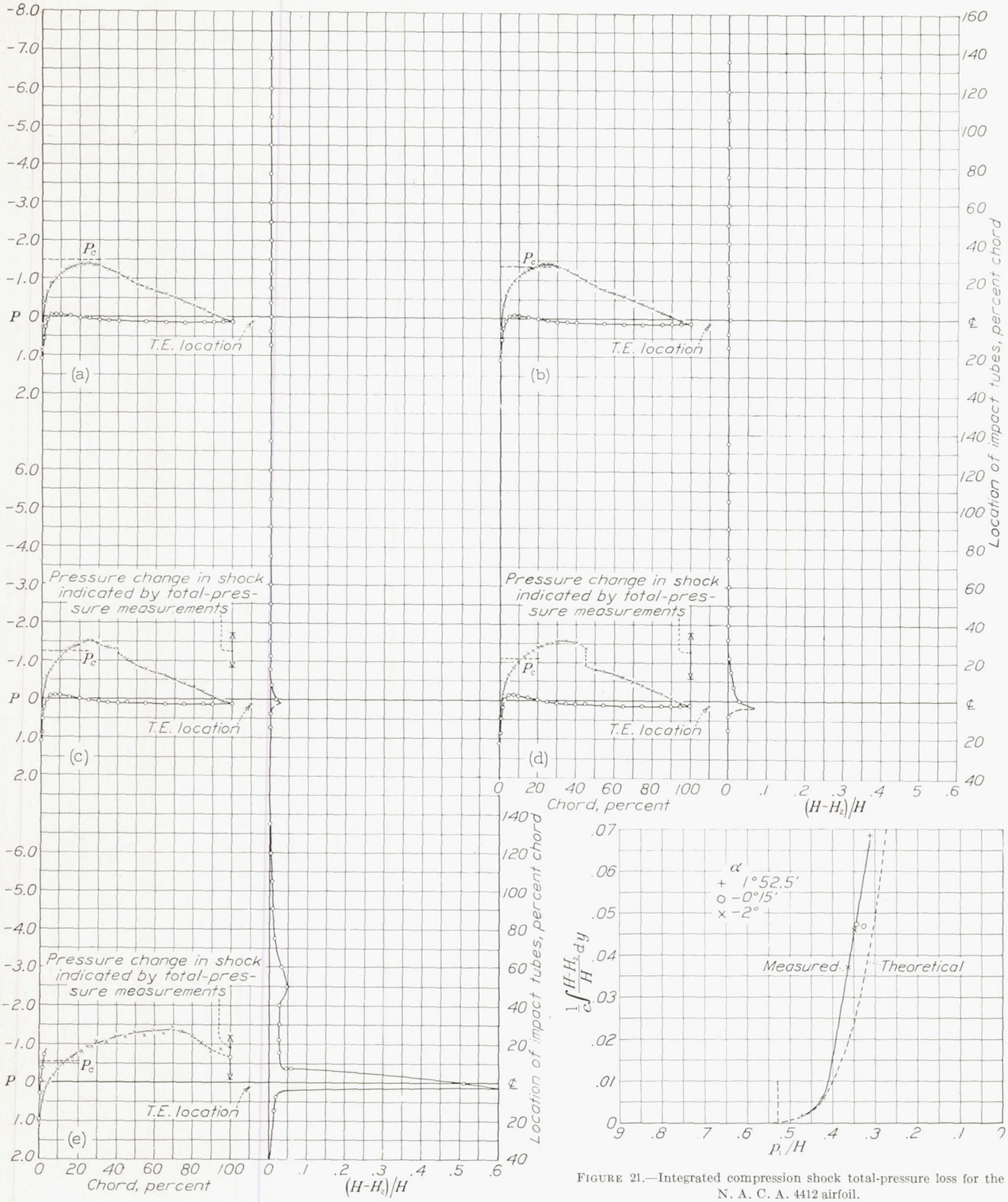

(a) $M=0.579$; test 24–27.
(c) $M=0.612$; test 24–27.
(e) $M=0.776$; test 24–27.

(b) $M=0.590$; test 24–27.
(d) $M=0.640$; test 24–27.

FIGURE 20.—Pressure distribution and compression shock total-pressure loss for the N. A. C. A. 4412 airfoil. $\alpha=1°52.5'$.

FIGURE 21.—Integrated compression shock total-pressure loss for the N. A. C. A. 4412 airfoil.

kinetic energy dissipated in the shock. Considerable further investigation appears necessary before complete understanding of the compressibility-burble phenomenon can be achieved.

THE CRITICAL SPEED

It is apparent from the preceding discussion that the most important detrimental effects arising from compressibility phenomena do not appear until the critical speed is reached. It is important to know the value of the critical speed for many applications, such as propeller problems and future high-speed aircraft, particularly those designed to operate at altitudes where, owing to the low temperature, the speed of sound is low. The theory thus far developed is not explicit and the first work of consequence was the electric analogy used by G. I. Taylor (references 13 and 14). From this method Taylor found that, when approximately the local speed of sound was attained, the theoretical potential flow failed. Further analytical examination (references 15 and 16) indicated that certain hypothetical flows could exceed the speed of sound without compression shock but by only a few percent. For engineering approximation, this work indicates that the critical speed can be taken as the value of the translational velocity at which the sum of translational and induced velocities equals the local speed of sound.

This assumption is substantiated, in general, by the data reported herein. The kinetic-energy-loss data, nearly all of the pressure-distribution data, and the total-pressure measurements indicate that the compressibility burble occurs when the local speed of sound is reached or only slightly exceeded. Using this assumption and the relation

$$P=\frac{P_0}{\sqrt{1-M^2}}$$

where P_0 is the incompressible or low-speed local-pressure coefficient, Jacobs, by placing P equal to the value corresponding to the speed of sound, devised a relation for the critical speed. (See reference 2.) The curve derived is given in figure 22. The abscissas are the low-speed or incompressible-flow values of the local-pressure coefficients and the ordinates are the critical-speed indices. A variation of this curve with abscissas equal to the thickness-chord ratios for elliptic cylinders is given in reference 17. For purposes of comparison, however, Jacobs' original curve is given. Results from these and other experiments are shown as the plotted points. The points shown for the circular cylinder are based on Stanton's pressure-distribution experiments (reference 18) and potential-flow theory, and the critical speed is based on low Reynolds Number experiments in the 11-inch high-speed wind tunnel.

All the experimental results indicate lower critical speeds than shown by the curve. The airfoil data for conditions in which the maximum negative pressure occurs near the nose indicate lower critical speeds than the other airfoil data. The reason for the difference is the underestimation of the compressibility effect by the theoretical term $1/\sqrt{1-M^2}$, a detailed discussion of

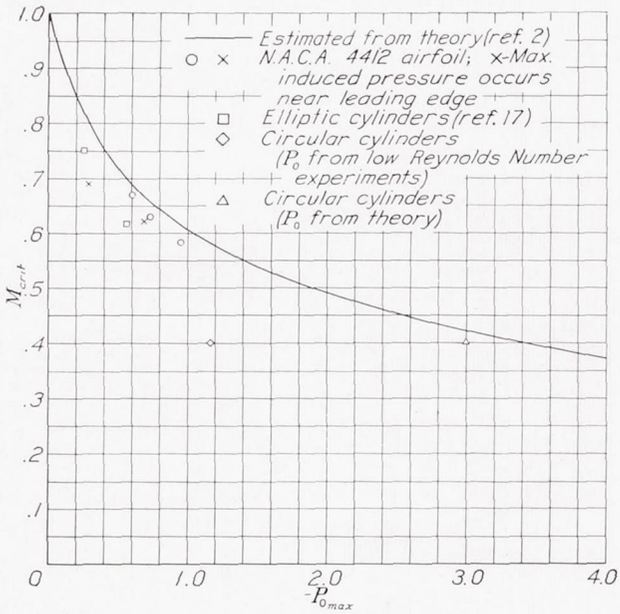

FIGURE 22.—Critical-speed ratio for various values of the maximum induced pressure reduction for compressible flow.

which has previously been given. From the variation shown by the curve and the experimental points, however, reasonably accurate estimates of the critical speed may be obtained for flows approximating two-dimensional conditions.

CONCLUSIONS

1. The physical nature of the flow change called the compressibility burble is shown. The large drag increments occurring at high speeds are associated with the kinetic-energy losses caused by a compression shock and these losses appear in the flow as decreased total pressure.

2. The theoretical information available is applicable only for speeds below the critical, that is, below the speed at which the compression shock forms; and, even in this range, the theory appears greatly to underestimate the compressibility effect for certain conditions.

3. The data permit a reasonably accurate estimation of the critical speeds for approximately two-dimensional flows.

4. Further theoretical study and experiment are desirable to enable more accurate prediction of the critical speed for two-dimensional flow and an extension of the present knowledge to three-dimensional conditions. The fundamentals of the disturbed flow should be further investigated experimentally to determine completely the nature of the actual flow from which it may be possible to effect a delayed compressibility burble.

LANGLEY MEMORIAL AERONAUTICAL LABORATORY,
NATIONAL ADVISORY COMMITTEE FOR AERONAUTICS,
LANGLEY FIELD, VA., *July 6, 1938.*

REFERENCES

1. Stack, John: The Compressibility Burble. T. N. No. 543, N. A. C. A., 1935.
2. Jacobs, Eastman N.: Methods Employed in America for the Experimental Investigation of Aerodynamic Phenomena at High Speeds. Misc. Paper No. 42, N. A. C. A., 1936.
3. Stack, John: The N. A. C. A. High-Speed Wind Tunnel and Tests of Six Propeller Sections. T. R. No. 463, N. A. C. A., 1933.
4. Wood, Robert W.: Physical Optics. The Macmillan Co., 1919, pp. 94–98.
5. Pinkerton, Robert M.: Calculated and Measured Pressure Distributions over the Midspan Section of the N. A. C. A. 4412 Airfoil. T. R. No. 563, N. A. C. A., 1936.
6. Jacobs, Eastman N., and Abbott, Ira H.: The N. A. C. A. Variable-Density Wind Tunnel. T. R. No. 416, N. A. C. A., 1932.
7. Glauert, H.: The Effect of Compressibility on the Lift of an Aerofoil. R. & M. No. 1135, British A. R. C., 1928.
8. Ackert, J.: Über Luftkräfte bei sehr grossen Geschwindigkeiten insbesondere bei ebenen Strömungen. Helvetica Physica Acta, vol. I, Fasciculus Quintus, 1928, pp. 301–322.
9. Theodorsen, Theodore: Theory of Wing Sections of Arbitrary Shape. T. R. No. 411, N. A. C. A., 1931.
10. Kaplan, Carl: Two-Dimensional Subsonic Compressible Flow past Elliptic Cylinders. T. R. No. 624, N. A. C. A., 1938.
11. Pinkerton, Robert M.: The Variation with Reynolds Number of Pressure Distribution over an Airfoil Section. T. R. No. 613, N. A. C. A., 1938.
12. Stodola, A.: Steam and Gas Turbines. Vols. I and II. McGraw-Hill Book Co., Inc., 1927.
13. Taylor, G. I., and Sharman, C. F.: A Mechanical Method for Solving Problems of Flow in Compressible Fluids. R. & M. No. 1195, British A. R. C., 1929.
14. Taylor, G. I.: Report on Progress during 1927–28 in Calculation of Flow of Compressible Fluid, and Suggestions for Further Work. R. & M. No. 1196, British A. R. C., 1929.
15. Taylor, G. I.: The Flow of Air at High Speeds past Curved Surfaces. R. & M. No. 1381, British A. R. C., 1930.
16. Taylor, G. I.: Some Cases of Flow of Compressible Fluids. R. & M. No. 1382, British A. R. C., 1931.
17. Lindsey, W. F.: Drag of Cylinders of Simple Shapes. T. R. No. 619, N. A. C. A., 1938.
18. Stanton, T. E.: On the Effect of Air Compression on Drag and Pressure Distribution in Cylinders of Infinite Aspect Ratio. R. & M. No. 1210, British A. R. C., 1929.

U. S. GOVERNMENT PRINTING OFFICE: 1939

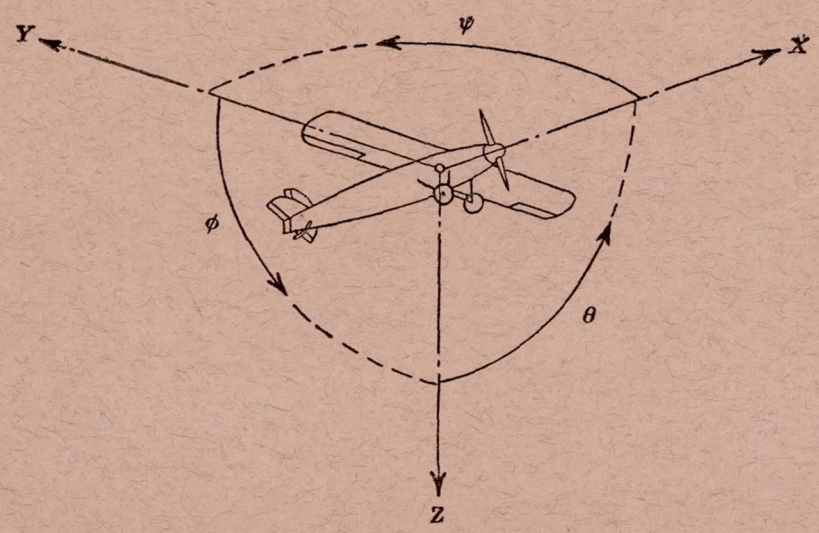

Positive directions of axes and angles (forces and moments) are shown by arrows

Axis		Force (parallel to axis) symbol	Moment about axis			Angle		Velocities	
Designation	Symbol		Designation	Symbol	Positive direction	Designation	Symbol	Linear (component along axis)	Angular
Longitudinal	X	X	Rolling	L	$Y \longrightarrow Z$	Roll	ϕ	u	p
Lateral	Y	Y	Pitching	M	$Z \longrightarrow X$	Pitch	θ	v	q
Normal	Z	Z	Yawing	N	$X \longrightarrow Y$	Yaw	ψ	w	r

Absolute coefficients of moment

$C_l=\frac{L}{qbS}$ (rolling) $\quad C_m=\frac{M}{qcS}$ (pitching) $\quad C_n=\frac{N}{qbS}$ (yawing)

Angle of set of control surface (relative to neutral position), δ. (Indicate surface by proper subscript.)

4. PROPELLER SYMBOLS

D, Diameter

p, Geometric pitch

p/D, Pitch ratio

V', Inflow velocity

V_s, Slipstream velocity

T, Thrust, absolute coefficient $C_T=\frac{T}{\rho n^2 D^4}$

Q, Torque, absolute coefficient $C_Q=\frac{Q}{\rho n^2 D^5}$

P, Power, absolute coefficient $C_P=\frac{P}{\rho n^3 D^5}$

C_s, Speed-power coefficient$=\sqrt[5]{\frac{\rho V^5}{P n^2}}$

η, Efficiency

n, Revolutions per second, r.p.s.

Φ, Effective helix angle$=\tan^{-1}\left(\frac{V}{2\pi r n}\right)$

5. NUMERICAL RELATIONS

1 hp.=76.04 kg-m/s=550 ft-lb./sec.
1 metric horsepower=1.0132 hp.
1 m.p.h.=0.4470 m.p.s.
1 m.p.s.=2.2369 m.p.h.

1 lb.=0.4536 kg.
1 kg=2.2046 lb.
1 mi.=1,609.35 m=5,280 ft.
1 m=3.2808 ft.

AUG 5 1970